Nanostructure technology

by T. H. P. Chang

D. P. Kern

E. Kratschmer

K. Y. Lee

H. E. Luhn

M. A. McCord

S. A. Rishton

Y. Vladimirsky

The ability to fabricate structures with lateral dimensions in the sub-100-nm range has opened a new field of research. This paper first reviews recent advances in nanolithography techniques, with a brief discussion of their relative merits and fundamental limits. Special emphasis is given to the scanning electron-beam method, which is the most widely used nanolithography method at the present time. The two main areas of nanostructure research are device technology and basic science. Highlights of a number of exploratory programs in these two areas are presented.

Introduction

The objective of research in nanostructure technology [1-10] is to explore the basic physics, technology, and applications of ultrasmall structures and devices with dimensions in the sub-100-nm regime. This work has two main components. First, there is the exploration of nanolithography techniques and the study of their fundamental and practical limits. Second, there is the application of the nanolithography techniques to the fabrication of a broad range of microstructures and devices and the conduction of basic research on these structures. In some cases, the feature size

[®]Copyright 1988 by International Business Machines Corporation. Copying in printed form for private use is permitted without payment of royalty provided that (1) each reproduction is done without alteration and (2) the *Journal* reference and IBM copyright notice are included on the first page. The title and abstract, but no other portions, of this paper may be copied or distributed royalty free without further permission by computer-based and other information-service systems. Permission to *republish* any other portion of this paper must be obtained from the Editor.

of these structures becomes comparable to the characteristic lengths associated with the elementary processes in physics, and simple structures can be used to obtain new insight into the quantum transport mechanisms and physical properties of materials. In other cases, complex structures will be needed to explore limits and feasibilities of future-generation solid-state devices. This paper discusses some of the recent advances in these two main areas of nanostructure technology.

1. Nanolithography

Nanolithography [11-19] is a relatively new extension of high-resolution lithography technology; it generally refers to the regime of linewidths less than or equal to 100 nm. In this regime, the choices of lithographic methods become very limited. For pattern generation, which is needed for direct write and mask-making, the scanning electron-beam method is by far the most widely used approach, with the scanning ion beam emerging recently as a possible alternative for some applications. New approaches based on the scanning tunneling microscope (STM) and the scanning X-ray microscope principle may prove important in the future. For pattern transfer using a mask, X-ray contact printing, electron-projection printing, and ion-projection printing are the options available. It is fair to say that for lithographies in the submicron (0.5- μ m to 1- μ m linewidths) and the deep submicron (0.1-μm and 0.5-μm linewidths) regimes, the key issues for the different methods are reasonably well defined. In the case of the electron-beam method, the issue for these regimes is mainly one of throughput and cost. This is not the case for the nanolithography methods. Here, because of its exploratory nature, the key issues are much less well defined.

In the deep-nanometer (≤10 nm) regime, the issues are mainly ones of establishing basic feasibility, with major difficulties arising from both system and process; in the regime closer to 100 nm, accuracy, resolution, and throughput issues are all important.

Because the electron-beam nanolithography method [20–34] plays an important role in nanostructure fabrication, the design considerations and practical performance of such a system are discussed first. This is followed by a discussion of the various other lithography methods available for nanostructure fabrication.

Electron-beam nanolithography

Scanning electron-beam lithography is the highest-resolution method for direct pattern generation. In this approach, the pattern is written with a small electron beam, which is controlled (deflected and turned on and off) by a computer. While a variety of electron-beam systems have been developed for lithography applications since the 60s and 70s, most of these are designed for submicron and deepsubmicron resolution. Their electron-optical performance as well as electrical and mechanical noise properties are significantly worse than the requirements for nanolithography. For this reason, much of the early work on nanolithography was performed using modified SEMs and STEMs. Although these instruments are well suited for this type of work from the point of view of beam size, their mechanical and electrical stabilities are often not adequate, and their electron-optical properties impose a severe limitation on field size. Broadly speaking, electron-beam systems have two major components: the beam-forming and beam-deflection system, and the pattern-generation and pattern-control systems. The more stringent requirements for nanolithography applications occur in the beam-forming and beam-deflection system.

Beam formation

Beam-forming systems for electron-beam lithography use either a Gaussian round-beam approach or the shaped-beam approach. At this point, the Gaussian approach which uses the conventional probe-forming concept of the scanning electron microscope is the system most widely used for nanolithography. In general, two or more lenses focus the electron beam onto the surface of the workpiece by demagnifying the electron gun source. High flexibility can be achieved, since the size and energy of the final beam can be readily varied by changing the focal length of the electron lenses and the accelerating potential of the electron gun. To ensure good line definition, the beam size is generally adjusted to a fraction, usually a quarter, of the minimum pattern linewidth.

The optical properties of the Gaussian beam system in the nanometer regime are determined by a combination of lens and deflection aberrations, diffraction, and source brightness [35, 36]. In the axial position, the principal aberrations are spherical, chromatic, and diffraction. When the beam is deflected off-axis, additional aberrations (transverse chromatic, coma, astigmatism, and field curvature) are introduced. The final beam diameter is given by a combination of these two main groups of aberrations. To improve resolution, it is necessary to reduce the axial aberrations, which necessitates the use of a short working distance in the final lens. A short working distance leads, however, to an increase in the deflection aberrations. The design of the system therefore requires careful trade-off and optimization of a multitude of parameters. In practice, most nanolithography systems today use the Gaussian optics to form a beam on a workpiece which is located outside the final lens to accommodate large workstage motions and ease of sample handling. In these systems, chromatic aberration generally dominates the axial aberrations. A typical system with a working distance of around 1 cm (a practical limit set by mechanical considerations) using a LaB₆ gun [37, 38] at 25 kV, can form a minimum axial beam diameter of approximately 5 nm. This fundamental limit is set by chromatic and diffraction effects. As the beam size approaches this limit, both the beam current and the current density decrease drastically due to the effect of the aberrations. Therefore, in practice, for such a system to operate at a reasonable stepping rate to satisfy throughput requirements, a practical minimum beam-diameter limit is set by the need to achieve some minimum level of beamcurrent density. Stepping rates of the order of a few MHz to expose a resist material such as PMMA, with a sensitivity of approximately 100 µC/cm² for nanolithography, require a current density of the order of several hundreds of A/cm². This requirement sets a practical minimum beam size for these systems to around 7 to 8 nm. These limits can be improved by increasing the beam-accelerating potentials. With a field-emission source [39-41], the higher brightness and lower energy spread of the source allow the same system to achieve a limit in minimum beam size of approximately 1 nm, with a current density in excess of 1000 A/cm² at this beam size. This significant advantage of a field-emission source over the LaB, source has been known for quite some time; it is not widely practiced mainly because of concerns over the stability and noise issues associated with such a source. Recent advances in thermionic field-emission (TFE) sources [42-48] based on either zirconiated tungsten or titanium tungsten emitters have increased the stability to practical levels. Further improvement in the beam size limits will require the workpiece to be immersed in the final lens, as in the case of the STEMs.

The design of deflection systems with minimum aberrations remains a difficult task, although some design optimization for both magnetic and electrostatic deflectors in the presence of a lens field can now be achieved through computer-assisted design programs [49–52]. Sophisticated

pre-lens deflection systems using two, three, and four tiers of deflectors [53–56] have been developed. It is conceivable that, in the future, a system using a thermionic field-emission source at ≥100-kV potentials and a VAIL-type [55, 56] deflection system with the workpiece located inside the final lens may be the solution to a sub-1-nm system with a wide-field-coverage capability.

Round-beam systems based on critical [57] and Koehler [58] illumination principles have also been developed. They offer some improvement in sharpness of beam profile over the Gaussian beams, but the basic design considerations are not significantly different.

Throughput of round-beam systems is determined by 1) the exposure time, which is governed by the beam-stepping rate, and 2) overhead times, which are the settling times for addressing shapes, registration, and stage move times, etc. At the present time, throughput is dominated primarily by the exposure time, with typical stepping rates in the few-MHz regime. This is in part due to brightness/beam-current limitations and partly due to slow resist materials used. With improvements in beam current with brighter sources such as the TFE source, and faster resist, improvement of stepping rates into the hundreds-of-MHz regime might now be possible. This will require an improvement in the deflection system and electronic driving units to operate at these speeds. Several high-speed deflection systems [27, 48] with performance ≥100 MHz have been reported, and they are significant achievements for the improvement of throughput. It should be pointed out that, as a general rule, electronic noise increases with speed, and the effect of this on pattern definition needs to be carefully assessed. Further improvements in round-beam throughput can be achieved by the "multiple beam size" technique [59], in which a smaller beam is used for fine lines and the critical edges and a larger beam is used for the coarse lines and fill-in of large areas.

The shaped-rectilinear-beam approach [60-62] offers the advantage of higher throughput than the round-beam approach. In this system, a rectangular beam is formed by overlapping the images of two square apertures in the electron-optical column. By varying the amount of this overlap, a variably shaped rectangular beam can be formed. Such systems have been successfully developed and used for lithography applications in the submicron and deepsubmicron regimes. Its application has, however, not yet been extended to nanometer resolution, probably for reasons of cost and complexity. The enhancement in throughput is achieved by having a higher average current—a typical shape may represent tens of the round-beam pixels. Fundamental limits in resolution, measured as the beam-edge sharpness in this case, are not significantly different from those of the Gaussian-beam case. Although electron-electron interactions [63, 64] can cause additional aberrations for applications in the submicron regime, this effect is probably not as severe

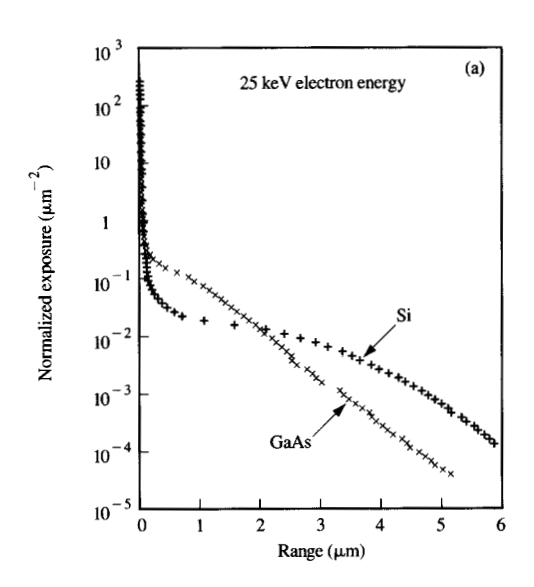
for nanometer applications, in particular for higher beam energies. A problem with shaped-beam systems is that they are not as flexible in generating angled lines and other nonrectangular shapes. Although in principle this problem can be solved by using apertures with complex shapes, the choices will invariably be restrictive. As throughput will in time inevitably become a critical issue, the variably shaped beam system offers a solution to this problem.

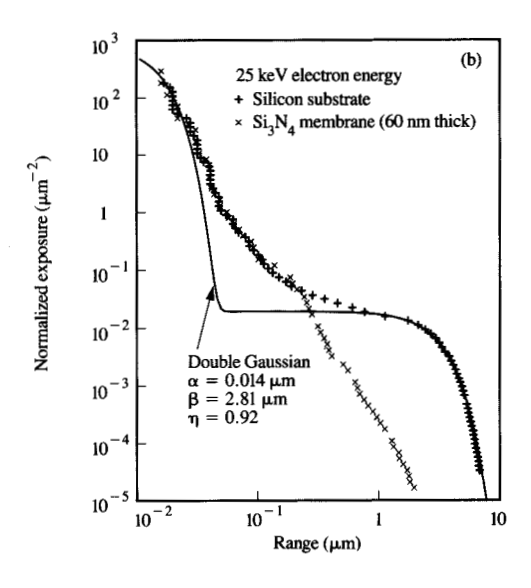
Pattern-generation and proximity effects

The two basic pattern-generation techniques are raster and vector. For nanolithography, vector scan is the method of choice primarily by reason of proximity-effect correction [65, 66], though other advantages such as higher exposure efficiency and improved data compaction are also important. Proximity effects are created by forward-scattered electrons in the resist and backscattered electrons from the substrate, which partially expose the resist up to several microns from the point of impact. As a result, serious variations of exposure over the pattern area occur when pattern geometries fall below the 1-µm range. Correction for these effects can be readily achieved in vector scan by adjusting the beam-stepping rate and hence the exposure intensity for each pattern element. A corresponding raster-scan-correction method based on a second compensating exposure step, the "GHOST" method [67], has been proposed. While this may be applicable to corrections for submicron patterns, its applicability for nanometer patterns is questionable because the effect of forward scattering cannot be corrected.

A technique has been developed [68], using a very-high-contrast resist, whereby the normalized point exposure distribution can be measured experimentally, both on solid substrates which cause backscattering and on thin substrates where backscattering is negligible. The data sets so obtained can be applied directly to proximity correction, and represent the practical conditions met in pattern writing.

Electron exposure is usually modeled by assuming that the total exposure distribution is given by the sum of two Gaussian distributions [65]. The first Gaussian results from the beam diameter and forward scattering. The second Gaussian results from backscattering. For nanometer patterns, the correction requirements become more stringent, and a more accurate understanding of the exposure distribution is important. For some materials an additional exponential term must be added to the Gaussian terms to obtain a better fit with the measured exposure profiles. In the exposure distributions obtained on silicon, gallium arsenide, and thin silicon nitride substrates, significant deviations from the commonly assumed double Gaussian distributions are apparent. On GaAs substrates, the backscatter distribution cannot adequately be described by a Gaussian function [see Figure 1(a)]. Even on silicon a significant amount of exposure is found in the transition region between the two Gaussian terms [Figure 1(b)]. This





Measured point exposure distributions: (a) on silicon and gallium arsenide; (b) on solid silicon and thin silicon nitride, compared to a double Gaussian distribution [68].

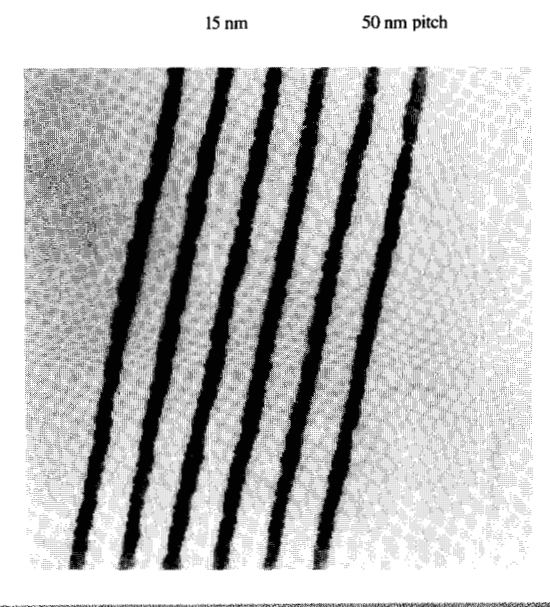
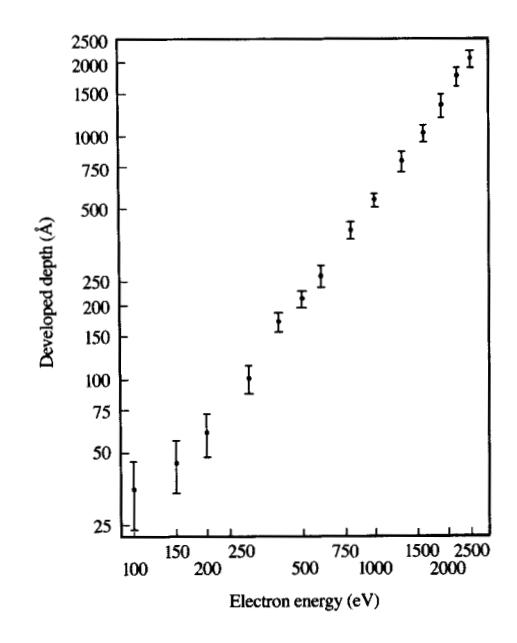


Figure 2

15-nm-wide gold palladium lines, 50-nm period, fabricated by lift-off on a thin silicon nitride membrane. Structures such as this have been fabricated in our laboratory as resolution test and calibration samples for X-ray microscopy (both scanning and replication techniques), and for atomic force and tunneling microscopy.



Figures

Plot of developed depth at 5 • 10⁻⁵ C/cm² exposure against electron energy [91].

Table 1 Parameters for the approximation of exposure distributions on silicon and gallium arsenide by double Gaussian and exponential terms. (Except for one data point, the resist thickness is <0.5 μm.)

Substrate Energy (keV) Silicon 25		Approximation	α (μm)	β (μm)	η	γ (μm)	ν	
		Double Gaussian	0.014	2.81	0.92			
Silicon	50	Double Gaussian	0.033	8.80	0.75	_	_	
10 μm AZ on Si	25	Double Gaussian	0.020	5.22	0.35		_	
GaAs	25	Double Gaussian	0.017	1.21	3.24	_	_	
GaAs	25	Gaussian + exponential	0.014	_	_	0.57	2.52	
GaAs	50	Double Gaussian	0.013	3.28	1.07	_	_	
GaAs	50	Double Gaussian + exponential	0.013	3.78	0.75	1.28	0.54	

exposure, which can be due to non-Gaussian tails in the primary beam and to forward scattering in the resist, must certainly be taken into account for accurate proximity correction in lithography on a sub-100-nm scale, and also at larger dimensions. The modified Gaussian proximity equation used to fit the experimental data is

$$f(r) = \frac{1}{\pi(1+\eta+\nu)} \left[\frac{1}{\alpha^2} \exp\left(-\frac{r^2}{\alpha^2}\right) + \frac{\eta}{\beta^2} \exp\left(\frac{-r^2}{\beta^2}\right) + \frac{\nu}{2\gamma^2} \exp\left(\frac{-r}{\gamma^2}\right) \right], \tag{1}$$

where α is the half-width of the forward-scattering Gaussian profile; β is the backscattered Gaussian profile half-width, and γ is the decay constant for the exponential term. η is the ratio of the backscattered to the forward-scattered intensity, and ν is similarly the ratio of the exponential term intensity to the forward-scattered intensity. **Table 1** summarizes the parameters that best fit the exposure profiles obtained from these measurements.

Resists and resolution limits

At an early stage in the development of scanning electron microscopy (1960), it was demonstrated that patterning of a thin membrane (in this case collodion) could be achieved with a resolution of about 20 nm [69]. In 1965 250-nm-wide metal lines were fabricated on a solid silicon substrate by the beam-induced polymerization of organic contamination (residual vacuum pump oil) onto the specimen and subsequent ion etching [70]. By using the same approach, 80-nm-wide aluminum lines were fabricated by chemical etching in 1967 [71]. A similar technique was later used to achieve 8-nm metal features on thin silicon nitride substrates [72]. Organic contamination as an electron resist suffers from very poor sensitivity (\simeq 1 C/cm²) and from depletion when closely spaced features are attempted.

The use of polymethyl methacrylate (PMMA) as an electron-beam resist [73] has led to more practical nanolithography. Exceptionally high resolution down to the order of 10-nm linewidth can readily be achieved [74, 75]. Although the resist sensitivity is not high, typically about 100 μ C/cm² for nanolithography, PMMA materials over a wide

range of molecular weights are available with reproducible characteristics. The highest-resolution metal lines that are essential to many of the nanostructure experiments have been fabricated almost exclusively by the lift-off process using this resist. In this case, a double-layer resist structure (to provide a controlled undercut profile) is often used to give the best results [74, 76].

Negative resists usually suffer from loss of resolution due to swelling; however, a polystyrene p-chlorostyrene copolymer [77] has been found to give about 20-nm resolution at a sensitivity of about 200 μ C/cm², and has been used for the etching of sub-0.1- μ m structures [78].

The amorphous nature of the inorganic resists arsenic trisulphide and germanium selenium glass has aroused interest in these materials for nanolithography, but the results from these materials have not approached the resolution of PMMA [79, 80], and their sensitivity is poor ($\approx 1 \text{ C/cm}^2$). Langmuir-Blodgett films have been patterned with fine lines as narrow as 10 nm [81] with a sensitivity comparable to that of PMMA.

Very fine, high-current-density electron beams have been used to cut 2-nm-wide lines through thin crystals of sodium chloride [82], lithium fluoride [83], and various metal beta-aluminas [84]. The direct electron-beam etching technique without a development step (sensitivity $\simeq 0.1 \text{ C/cm}^2$) necessitates much longer exposure times than conventional exposure-development techniques. Patterns cut in these materials have been successfully transferred from these materials to semiconductor materials using reactive ion etching [83, 85].

On thick substrates, the resolution of PMMA for isolated lines or sparse patterns is about the same as that on thin-membrane substrates. At 50 keV [86], 8-nm-wide lines in resist have been achieved. However, for dense patterns the resolution is generally poorer than on thin membranes due to a reduction in contrast by significant backscattering of high-energy electrons from the substrate [87]. Closely spaced metal lines of 30- to 40-nm linewidths have been achieved by lift-off using a 50-keV electron beam [12]. With higher electron acceleration potentials (≥120 keV), the backscattered electrons are spread over tens of microns;

then, by writing patterns of a few square microns in total area (much less than the backscattering range), it has been possible to reduce the effect of electron scattering to such an extent that 10-nm-linewidth dense patterns have been achieved on solid gallium arsenide [88].

On thin-membrane substrates, the improved contrast with the absence of backscattered electrons enables smaller and denser structures to be defined, and it has been possible to achieve closely spaced metal lines 10 nm wide [74]. Figure 2 shows as an example 15-nm-wide gold palladium lines fabricated by lift-off in PMMA on thin membrane. Double-layer PMMA was used in this experiment, the bottom layer being 35 nm thick and the top layer 25 nm thick.

The thin-substrate results naturally lead to the question: Why is the resolution of PMMA limited to about 10 nanometers? It has been suggested that secondary electrons produced by the inelastic collisions of the primary (i.e., incident) electrons play a significant role in limiting the resolution. Some suggested that fast (keV) secondary electrons are important because they have longer ranges than lower-energy electrons [89]; however, this theory is questionable as an explanation for the ultimate resolution limit, since only relatively few high-energy secondaries are produced in high-resolution lithography on thin substrates. Elsewhere it has been proposed that, on the contrary, low-energy secondaries are more significant, since electrons of about 5 eV and above are able to expose the resist and may have ultimate ranges of the order of tens of nanometers [75].

Experiments were performed to measure the range over which low-energy electrons, from 5 to 2500 eV, are able to expose PMMA such that it will subsequently dissolve in developer [90, 91, 92]. The results are shown in Figure 3; it is seen that secondary electrons of 100 eV energy have less than 5-nm exposure range in the polymer. The numbers and energies of secondary electrons produced during exposure were also derived from electron energy loss spectra (EELS) measured in both PMMA and silicon nitride (the substrate material) [90, 92]. The experimental data were combined in a three-dimensional Monte Carlo program to simulate the linewidth-dose relationship for exposure by a very fine 100keV beam [90]. The results of the simulation are compared with experiment in Figure 4; at a line dose that results in the smallest experimental linewidth of 10 nm, the simulation shows that the secondary electron limit is much smaller (~2 nm). This indicates that most of the secondary electrons are too short-range an effect to be causing the minimum linewidth of 10 nm as observed.

The threshold molecular weight (number average) for entanglement of PMMA molecules is known from viscosity experiments to be about 16 000 [93]. Typical electron-beam exposure of du Pont Elvacite grade 2041 PMMA would reduce its number-average molecular weight from 186 000 to 3300 [90]; the transition through the entanglement threshold during exposure greatly increases the solubility of the

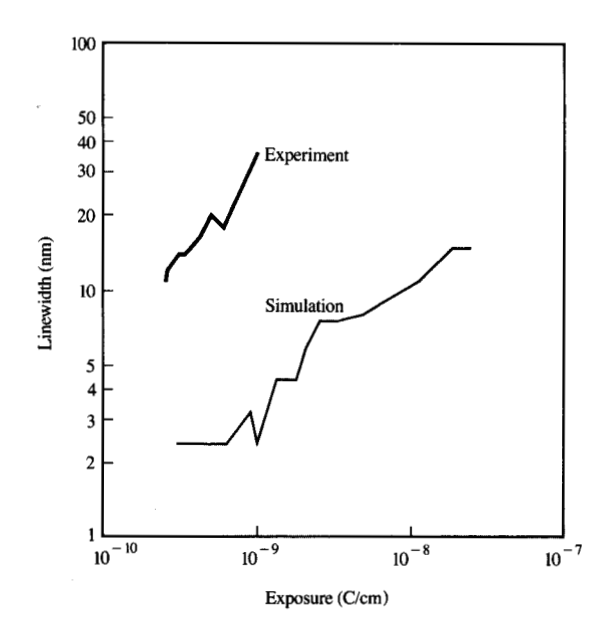


Figure 4

Experimental and simulated linewidth–exposure dose relationships for exposure by a very fine beam at 100 keV [90].

polymer and is thought to be partly responsible for the high contrast and resolution of PMMA. Below the entanglement threshold, the molecules of an undiluted polymer are configured similarly to those in a dilute solution [94], and one can assume that the individual molecule occupies its own roughly spherical volume with insignificant intrusion from its neighbors. A molecule of 16 000 molecular weight would contain 160 monomer units and occupy a sphere of about 4 nm diameter (the PMMA monomer contains 100 atomic mass units and the density of PMMA is 1.23 g/cm³). Such a molecule would dissolve much more rapidly than its entangled neighbors. It is reasonable to expect that a resist layer a few molecules thick would have a resolution limit of about twice this dimension, i.e., 8 nm, since the random arrangement of the molecules would prevent the opening of a vertical slot only one molecule wide. This model is proposed as a possible explanation for the resolution limit of PMMA, although the dynamics of swelling and dissolution during development are not taken into account.

Practical system performance

VS-6, an ultrahigh-resolution electron-beam vector-scan system dedicated to nanolithography, has been developed [18, 30]. The design is based on a vector-scan lithography system [36, 95, 96] with modifications to improve significantly the beam-forming and beam-deflection

Table 2 Design performance of the VS-6 lens-deflection system over a range of field sizes.

Beam voltage (kV) Energy spread (eV) Beam half angle (rad)	$ \begin{array}{c} 25 \\ 2.5 \\ 2.1 \times 10^{-3} \end{array} $,
Scan field (mm)	0.1	0.2	0.5
Spherical aberration (nm)	0.2	0.2	0.2
Axial chromatic aberration (nm)	4.1	4.1	4.1
Field curvature (nm)	4.0	16.1	100.0
Astigmatism (nm)	1.3	5.1	31.9
Coma (nm)	0.8	1.7	4.2
Transverse chromatic aberration (nm)	1.0	2.0	5.0
Total without dynamic correction (nm)	6.0	17.6	106.0
Total with dynamic correction (nm)	4.3	4.9	7.7
Distortion (nm)	1.3	10.2	161.0

Table 3 VS-6 performance: Measured data vs. design objectives.

	Theoretical	Measured (nm)	
Beam diameter (10 pA, 100 μm field			
size)	7.4 nm	8	
Electrical noise from deflection	<1/16384		
system	of field size	3.9	
Mechanical vibration interference		1.3	
Acoustic noise interference		< 0.1	
Magnetic interference (60 Hz and			
180 Hz)		3.7	

capabilities, and the noise, drift, and linearity characteristics of the deflection electronics; to provide a vacuum environment free of contamination; and to reduce the various resolution-limiting effects of electromagnetic interference and mechanical vibration.

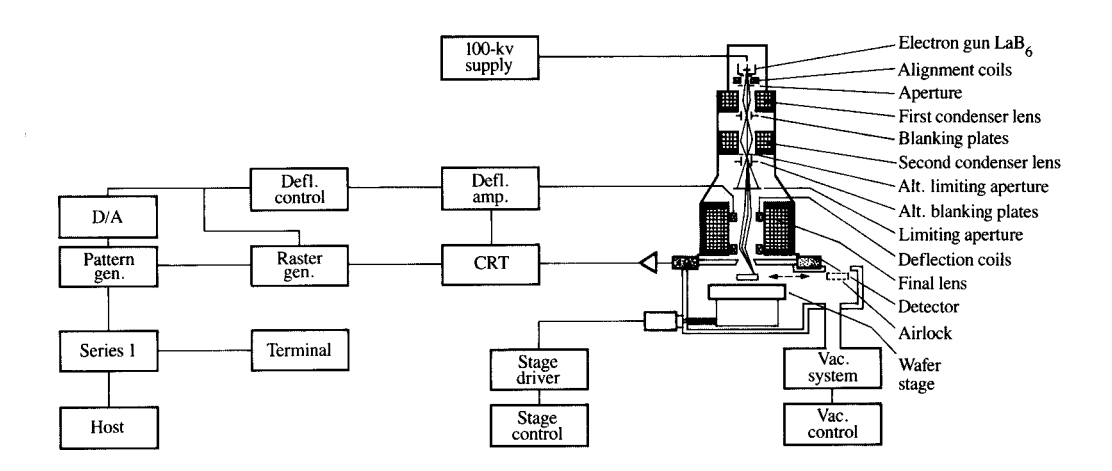
Figure 5 gives a schematic representation of the complete VS-6 system. It consists of a three-lens electron-optical column designed specifically for a minimum beam size of 5 nm and a deflection system optimized for a 20-nm beam over a 250-μm-square field. The performance of the beamforming and beam-deflection system for a sequence of field sizes is summarized in Table 2. A single-crystal LaB₆ electron-gun assembly is used to achieve a suitable current density for high-resolution resist with accelerating voltages from 10 to 100 kV. A compact four-quadrant solid-state detector is used for SEM and registration to overcome the geometric restriction imposed by the reduced working distance required to achieve the resolution improvement.

The pattern generation uses a 14-bit vector-scan exposure system with individual shape-to-shape dose variation as computed by the large database proximity-correction programs necessary for accurate shape definition at these dimensions. The system also has a polar-to-Cartesian converter to facilitate exposure of circular geometries.

The effective minimum spot size and the minimum feature size in an electron-beam lithography system depend on the characteristics of the electron-optical column and on the electrical and mechanical stability of the lithography system itself, as well as on the amount of environmental interference from mechanical, acoustic, and magnetic noise sources. The relevant points of interest are the beam diameter and the stability of the electron-beam position with respect to the substrate. Both parameters have been measured and characterized with an improved "edgemeasurement technique" [97] in which the electron beam is scanned across or is stationary at the edge of a suitable substrate, as illustrated in Figure 6. The transmitted electron signal is either analyzed on an oscilloscope or in a signal analyzer to determine parameters such as beam diameter or the magnitude and frequency spectrum of noise deflecting the beam. The resolution of this technique for measuring position instabilities proved to be well below 0.1 nm. Comparison of the data obtained from the edgemeasurement technique with the results of independent measurements, e.g., with a seismometer, is used to identify noise sources and establish their influence on the beam stability.

This measurement technique has been used to characterize the system with respect to the stability of its components and to interference from external noise sources such as mechanical, acoustic, and magnetic interference. The high resolution of this technique allows areas of system weakness to be clearly identified and the effectiveness of the corrective measures applied to be quantified. For mechanical vibration, by comparing frequency spectra from seismometer measurements to frequency spectra obtained from the edgemeasurement technique, it was found that while the pneumatic vibration isolation mounts provide good isolation of floor vibrations, the very low levels of mechanical vibrations left in the chamber can excite mechanical vibrations in the stage, which has several resonance frequencies between 29 Hz and 120 Hz. Thus, proper vibration damping in the stage is essential. To reduce further the impact of stage vibrations on the substrate stability with respect to the electron beam, a piezoelectric locking substage was designed to lock the substrate to the bottom of the objective lens, while at the same time providing vibration isolation between the x-y stage and the substrate. Magnetic interference was identified as a primary noise source for the system, and the effect was found to be primarily at 60 Hz and 180 Hz, originating in power line installations. To improve the magnetic shielding of the column, a "magnetic bottle" approach was implemented in which the final lens is magnetically separated from, but totally enclosed in, the outer shield.

Table 3 summarizes the system performance data after the implementation of most of the improvements described above. The comparison between the theoretical and the



Schematic diagram of the VS-6 electron-beam nanolithography system.

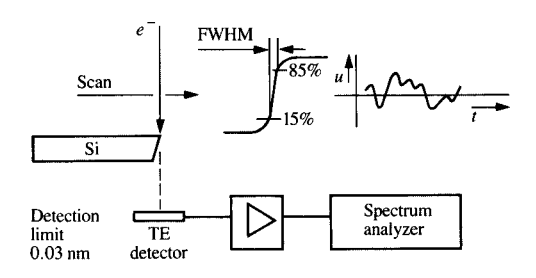
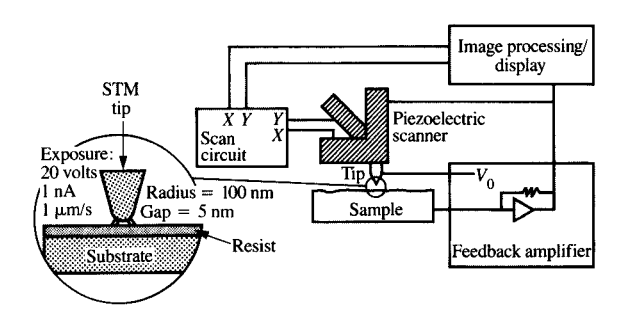


Figure 6

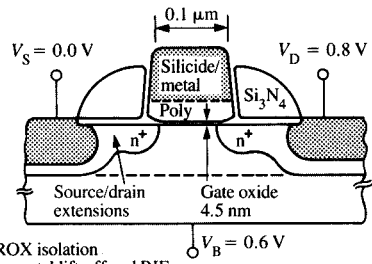
Schematic diagram of the edge-measurement technique.



 $A\,22\text{-nm-wide},\,12\text{-nm-thick line of gold-palladium transferred from}$ a PMMA resist pattern using lift-off technique. The resist pattern was made with the STM using a 20-V, 1-nA beam at a writing speed of I μm/s.



Schematic diagram of the scanning tunneling microscope showing its major components and some typical parameters used in STM lithography.



- 160-nm semi-ROX isolation
 Gate patterning: metal lift-off and RIE
 As/Sb source/drain extension
- Self-aligned silicidation of gate, source, drain Low-temperature passivation oxide Rapid thermal annealing extensively used

Figure 9

Schematic cross section of the NMOS device, with key design and process features.

469

measured values shows that the resolution is as close as possible to the limits imposed by the electron optics of the system, and interference from environmental noise sources is very low. It also demonstrates that it is possible to improve the system design to achieve adequate stability for nanometer resolution in a standard laboratory environment. At 25 kV, a beam diameter of 8 nm with a current of 10 pA has been achieved, which represents the practical limit intended for the system. Using this beam, 15-nm metal lines have been successfully fabricated using lift-off, as shown in Figure 2. The system has been used for a number of applications to be discussed subsequently.

• Other nanolithography methods

While scanning electron beam is the main method for nanolithography, several other methods are also available; their performance and status are discussed briefly here. Alternate pattern-generation methods based on focused ion beam, STM, and focused X-ray probe are discussed first. This is followed by mask-transfer methods using X-ray, electrons, and ions.

Direct pattern generation

Focused ion beam

A focused beam of ions can be formed and deflected in much the same way as an electron beam, and can be used for a wide spectrum of applications which include lithography, ion implantation, ion milling, and ion-beam-induced etching or deposition [98, 99]. The most widely used source is a liquid-metal Ga source, although other ion species (e.g., H, He, Be, B, Al, Si, P, As, In, Pd, and Au) can also be used. Several scanning ion-beam lithography systems with vector-scan pattern-generation capability have been developed, and their applications to nanolithography have recently been explored [100–104]. Patterns with 100-nm linewidth in PMMA resist have been achieved and, in one case, 30-nm-diameter dots of resist at 60-nm centers have been fabricated [101, 102].

The relatively large energy spread of 10–25 eV for most liquid-metal ion sources and alloy sources, together with the relatively large aberration coefficients of the ion-beam column, causes the minimum spot size to be chromatic-aberration-limited, thereby reducing the available current density at the substrate. The highest resolution yet obtained uses a Ga source, and a minimum spot size of 50 nm with a current of 10 pA has been achieved which represents a current density one to two orders of magnitude lower than in the electron-beam case based on a LaB₆ gun. Gaseous field-ionization sources offer a possibility of a higher source angular intensity of about 20 μ A/sr and a lower energy spread of about 4 eV, and thus increased current density in a nanometer spot size [105–107], but they are still in an early stage of development. Resist materials such as PMMA can

be used for ion-beam exposure, and their sensitivity is typically around 2 μ C/cm², which is one to two orders faster than for electron exposure. This means that the exposure speed of ion-beam systems can be very comparable to that of some of the electron-beam systems.

The ion beam is not expected to have as high an ultimate resolution as the electron beam (minimum spot size may be limited by aberrations to around 20 nm). In the case of Ga ions, the penetration range is relatively small and will require high accelerating potentials and/or multilayer resist systems. However, it has the advantage of not requiring proximity-effect corrections. In addition, it can be used for high-resolution milling, selective area implantation, and other applications not possible with electron beams. It therefore has an important role in nanostructure fabrication.

STM lithography

The scanning tunneling microscope [108] operates by positioning a very sharp tip (radius typically <100 nm) within a few angstroms of the surface using a threedimensional piezoelectric scanner. A voltage (typically <1 volt) is applied between the tip and the sample, causing a tunneling current to flow. A feedback amplifier monitors the current and adjusts the tip height to keep it constant. The tip is then scanned over the surface in a raster fashion, and the tip height is used to build an image of the surface topography, often with atomic resolution. Normal operation of the STM has little or no effect on the sample; however, by increasing the applied voltage to the point where the electrons have sufficient energy to cause a chemical reaction, and introducing an electron-sensitive material into the system, the STM is capable of performing nanolithography, as shown schematically in Figure 7.

Although the concept is relatively new, a variety of techniques have already been explored. One method uses the STM to expose very thin films (<20 nm) of various electronbeam resists, including contamination resist, Langmuir-Blodgett films, metal halide films, and PMMA polymer resist (Figure 8) [109]. Another technique is to use the STM to deposit metal directly from organometallic vapors that decompose on the surface when bombarded with electrons [110]. Also, bumps have been created on the surface of metallic glasses by thermally and electrostatically enhancing the surface diffusion of atoms underneath the tip [111]. All of these methods have achieved resolution ranging from 10 to 20 nm. Atomic-scale resolution has been achieved by pulsing the tip voltage to locally transfer individual atoms from the tip to atomically smooth crystals of germanium [112]. Finally, by substituting a liquid-metal ion source for the tip and reversing its polarity, submicron-diameter holes have been ion-milled in silicon and gallium arsenide substrates using ion energies as low as 100 eV [113].

The STM has a number of advantages over conventional electron beams, as well as some disadvantages. The current

density at the target is limited by destructive heating rather than by source brightness, and can be orders of magnitude higher than in conventional systems. The low-energy electrons eliminate the proximity effect caused by backscattered electrons, as well as any potential radiation damage to sensitive devices. However, the STM is limited to writing on conducting surfaces or surfaces with very thin insulating films. Also, the tip must be mechanically scanned over the surface at high speeds while maintaining tip-tosample separation with an accuracy of the order of 0.1 nm. While the needed accuracy is easily achieved with piezoelectric transducers, reaching speeds required for reasonable throughput will be more difficult. However, the STM has already been shown to be capable of fabricating nanometer-scale devices for research purposes [109]. For the future, it can be projected on the basis of theoretical calculations that a resolution of approximately 2 nm may be achievable using surface-acting mechanisms such as direct deposition and Langmuir-Blodgett films [114]. In addition, there is considerable interest in finding new techniques for fabrication at the atomic level, a regime inaccessible by any other current method.

Focused X-ray probe

The successful development of the scanning X-ray microscope [115] with sub-100-nm resolution suggests that it may be applicable also for nanolithography applications. In such a microscope, a coherent flux of X-ray in the energy level of about 400 eV ($\lambda=30$ A) is focused by a zone plate to form a diffraction-limited spot on a sample which is mechanically raster-scanned to form an image. A spot size of 75 nm has been achieved using a gold zone plate with minimum zone width of 50 nm with a depth of focus of 1 μ m. By replacing the sample with a resist-coated substrate and introducing a beam-blanking mechanism, lithography exposure can be performed. The lack of scattering in the resist allows sub-100-nm patterns with high aspect ratio to be generated directly without a mask.

The resolution of such a system is governed primarily by the resolution of the zone plate. It is reasonable to expect that zone plates with a sub-50-nm minimum zone width can be fabricated; thus, forming a spot of this order should be possible. The focal length of such a lens can be of the order of several millimeters, with several microns of depth of focus. The speed of the system will depend on the availability of X-ray flux. A synchrotron source with specially designed undulators and monochromators is needed to produce a highly coherent flux of 0.1% bandwidth. Based on the design data of two synchrotron sources [116] now under development, a flux in the focused spot of 50 nm diameter is estimated to be of the order of either 1×10^9 photons/s or 1×10^{12} photons/s, depending on the system selected. This estimate includes losses in the beamline of approximately 95% and a zone plate efficiency

of 5%. This translates into a dose per 50-nm pixel of 4×10^3 J/s/cm² and 4×10^6 J/s/cm², respectively. For a resist such as PMMA with a sensitivity of 500 mJ/cm², the pixel rate is calculated to be 8 kHz and 8 MHz, respectively. The higher value of pixel rate compares favorably with some of the scanning electron-beam systems today.

This approach has yet to demonstrate feasibility. Technical problems with beam blanking, sub-50-nm zone plate fabrication, etc. still need to be resolved, not to mention the availability of the source. Nevertheless, nanometer patterns with high aspect ratio and the ability to expose insulating samples without conductive coating are attractive.

Mask transfers

X-ray printing

Although the feasibility of the X-ray proximity printing method for submicron lithography has been established, its application to nanolithography is relatively new; much work remains to be done in optimizing the mask absorber and membrane, proximity gap and resist systems.

The most frequently used X-ray nanolithography systems employ an electron-bombardment X-ray source [117-119]. Using a 1-kW source at a distance of 100 mm from the mask, a power density of about 0.25 mW/cm² can be achieved at the mask, which leads to exposure times of one hour for PMMA resist. These sources emit a line spectrum in the wavelength range of 0.44 to 1.3 nm, characteristic of the target material. To minimize penumbral blurring and geometric distortions in high-resolution lithography, the gap between the wafer and the mask must be as small as possible, so contact printing is often employed. Contact X-ray lithography was used to produce minimum lines and spaces of 20 nm replicated in PMMA using a special mask made by shadow evaporation [120] and ~50-nm lines and spaces using electron-beam lithography for mask-making [121].

The delicate thin-membrane mask may easily be damaged during X-ray contact lithography and may contaminate the substrate during the exposure process. Therefore, for practical X-ray exposures, a small proximity gap between the mask and the wafer is required. A "microgap" technique in which a gap of a few microns is accurately controlled using studs has been proposed to facilitate alignment [121]. For this proximity printing method to achieve a resolution approaching 100 nm requires a submillimeter source size to reduce the penumbra effect. This may be obtained either from a laser-produced plasma source or an electrical discharge source with a source size of about 100 µm to 2 mm [122-124]. These pulsed sources emit a line spectrum and a low-intensity continuum in the wavelength range of 0.4 to 2 nm and produce a power density of about 10 mW/cm² at the mask. With a 200- μ m source size, a 3- μ m

proximity gap, and a 400-mm source-to-mask distance, the penumbral blurring can be reduced to 1.5 nm and can be neglected. However, in this case the minimum feature size is limited by Fresnel diffraction to approximately $1.5 \times$ $\sqrt{\lambda \times g}$, where λ is the wavelength and g the gap spacing. For the setup described, the minimum linewidth is limited to about 100 nm using a 1-nm wavelength [125, 126]. Fresnel diffraction is also the major resolution limitation for systems using synchrotron radiation [127-129]. The geometric distortion in systems using synchrotron radiation sources is less than 25 nm, since the beam divergence is less than 5 mrad and a source size is less than 0.5 mm [126]. In the resolution limit, it is the range of the photoelectrons which determines the edge sharpness and hence the finest linewidth. This range is about 40 nm for aluminum radiation ($\lambda = 0.83$ nm) and 5 nm for carbon radiation ($\lambda =$ 4.48 nm) [130]. For synchrotron radiation ($\lambda \simeq 1$ nm) this range is about 25 nm [126]. For high resolution it is obviously better to use softer radiation, but this requires a very thin mask which is difficult to handle and may not be dimensionally stable. Shorter wavelengths and thicker masks will give better mask stability, but the minimum linewidth is relatively large.

Electron-beam projection printing

Electron-beam projection systems have, potentially, higher throughput than scanning systems. However, their resolution is poorer than that of scanning systems, and they all share the same difficulty of not being able to correct for proximity effects. Three types of electron systems have been developed: the 1:1 photocathode projection, the shadow mask proximity projection, and the reduction projection.

The photocathode projection system [131, 132] uses ultraviolet light to irradiate a photocathode which is masked by a thin metal pattern, and the photoelectrons are accelerated to the wafer which acts as the anode. A uniform magnetic field focuses the electrons. The dominant aberration limiting resolution is chromatic aberration, and theoretical estimates of minimum linewidth vary from 1 µm to 100 nm. The minimum resolution achieved in this system is ~ 0.3 -µm lines and spaces, limited by the difficulties in mask-making and the lack of proximity-effect correction. Other difficulties include the absolute value and uniformity of the electric and magnetic fields, the substrate flatness requirements, and mask contamination resulting in a decay of the emission from the photosensitive layer. For these reasons, this method is not expected to be readily applicable for nanolithography.

In shadow-mask proximity printing, a shadow image of a transmission mask is projected onto a resist-coated substrate by scanning a 1-mm-diameter collimated electron beam with a mask-to-substrate gap of about 500 µm [133, 134]. The mask consists of a 2-µm-thick silicon stencil mask, and two complementary masks are used to facilitate the exposure of

ring-shaped structures. The substrate is mounted on a laser-interferometer-controlled x-y stage to allow for the stitching of complementary masks and for a step-and-repeat exposure process of the whole substrate. The electron-optical column operates at 10 kV and provides a high degree of flexibility for beam collimation and mask-to-wafer registration. The minimum linewidth achieved to date is about 0.5 μ m, although finer features approaching 100 nm have been shown. The application of this approach to nanolithography will require considerable effort in stencil mask development, and the accuracy of stitching of the complementary masks may also impose a limit.

The reduction projection systems [135-138] also use a stencil mask, which is illuminated by an electron gun and a condenser lens. A symmetric magnetic doublet lens together with an objective lens forms image of the mask on the substrate. The field size can be larger than that in a scanning system because the beam half-angle can be much smaller and off-axis aberrations are minimized. On-axis, the resolution is limited by the aberrations of the objective lens, which can be made small by reducing the focal length. Pattern lines of 40- to 50-nm linewidths in resist have been achieved using a system with a reduction of 120× [138]. To cover a field of reasonable size, off-axis aberrations due to coma, astigmatism, etc. have to be considered. Because these aberrations are sensitive to alignment accuracy of the complex electron-optical components of the column, they tend to cause serious limitations. Similar sensitivity to column alignment also exists for the pattern linearity, resulting in major difficulty with overlays in these systems. Various techniques to improve column alignment and to compensate for distortions have been proposed, but a practical system for lithography, either submicron or nanometer resolution, has yet to be developed.

Ion-beam projection printing

Protons are typically used in ion-beam projection systems, because they have the greatest range in resists. The resolution limit of ion-beam lithography is estimated to be less than 10 nm in PMMA for light ions, e.g., H. This limit is believed by many to be set by the range of the secondary electrons [139–141]; however, the earlier discussion on resolution limits in e-beam lithography may also apply here. Two types of ion-beam projection systems, the 1:1 shadow mask and the reduction projection, have been developed.

Shadow-masked ion-beam printing can be done with a broad collimated parallel beam of ions, with energies between 10 kV and a few hundred keV penetrating a mask in close proximity to a resist-coated substrate. Three types of masks have been used: 1) stencil masks, 2) thin amorphous masks with ion-stopping absorber patterns, and 3) thin single-crystal channeling masks with ion-stopping absorber patterns. The lifetime of the mask is limited less by effects from the ion exposure than by handling and contamination.

Stencil masks do not have a supporting membrane, and thus exhibit no ion scattering in the transparent regions of the mask [139, 142, 143]. However, they cannot be used with all kinds of patterns, e.g., ring-shaped patterns, unless more elaborate complementary-mask double-exposure techniques are used, which increases the alignment problems. For a good contrast between the mask material and openings in the mask, the openings have to be etched into the mask with a high aspect ratio (up to 10 for 0.5-\mumhigh and 50-nm-wide openings), or the mask has to be covered by an ion-stopping layer at the risk of additional mask distortion due to stress in the absorber layer. Features with minimum linewidth down to 20 nm have been replicated into PMMA resist using this technique and electron-beam lithography for mask-making [139]. Even with a mask-to-wafer proximity gap of 25 μm, 40-nm-wide lines were replicated into PMMA [143].

Membrane masks with absorber patterns have to be fabricated in such a way that the ion scattering in the transparent regions of the mask is minimized. This can be achieved by using materials composed of light elements such as boron nitride, silicon nitride, or aluminum oxide for the membrane. However, even with a membrane thickness of only 100 nm, ion-beam scattering in the membrane is significant and prohibits any significant proximity gap between the mask and the resist-coated substrate.

A better [144–146] approach is to minimize the scattering in the mask membrane by using silicon single-crystal material and taking advantage of the ion-channeling effect. In this case the ion beam must be aligned to the lattice of the thin single-crystal silicon membrane, resulting in a scattering angle of the ions of as low as 0.3 degree. Then the thickness of the membrane may be as much as $0.5 \mu m$, and still a proximity gap of about 25 μ m between the mask and the wafer can be used while obtaining 0.1- μm resolution. The absorber consists of a heavy element such as gold or tungsten. The gold may be patterned by sputter etching, although electroplating might be beneficial in fabricating patterns with <500-nm linewidth, high aspect ratio, and vertical walls as in X-ray lithography. At present, masked ion-beam lithography is geared toward 0.5-μm minimum feature size [146].

The basic features of an ion-beam reduction projection system are very similar to its electron-beam counterpart [147]. Therefore, much of the discussion and difficulties on the electron-beam case apply also to the ion beam. Since the ion optics must consist of electrostatic lenses or electrostatic and magnetic multipole lenses, which in most cases have optical properties inferior to the magnetic lenses for electrons, it will be more difficult to achieve high resolution. The absence of proximity effect for ion beams and the possibilities of high-throughput ion-beam processes, such as milling and direct implantation, may present some unique opportunities for this approach in nanometer resolution.

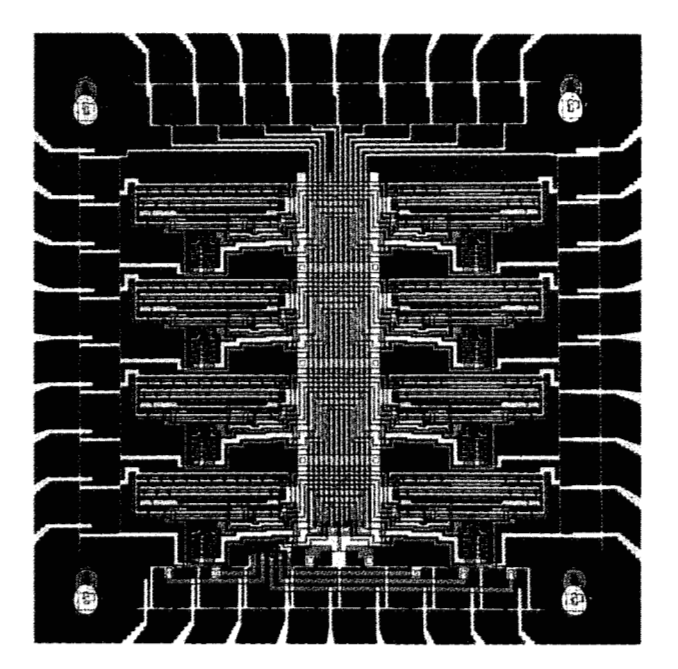
2. Nanostructures and devices

The two main areas of research in nanostructures are 1) ultrasmall devices for the investigation of fundamental limits and the exploration of new device concepts; and 2) basic science, which covers a wide range of topics from quantum transport, cryogenic tunneling, and small-particle arrays all the way to diffractive optics and molecular electronics. This section highlights some of the recent advances of a number of collaborative programs in our laboratory in these two areas. An important ingredient of many of these programs is the interdisciplinary nature of the effort. While nanolithography plays a key role, the other disciplines are equally indispensable.

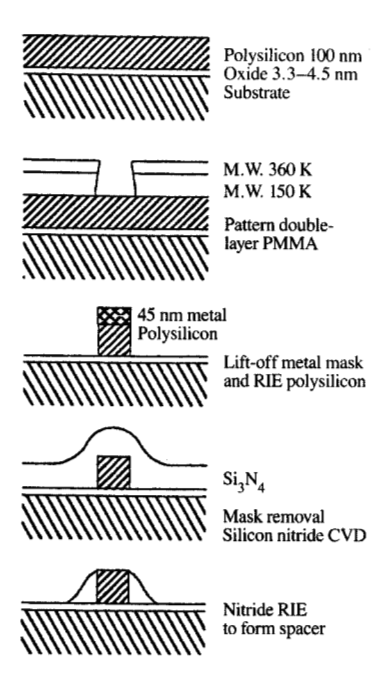
• Scaling of silicon MOSFETs

The most striking feature in Si-FET device and circuit development has been the progress in scaling of devices to ever-smaller dimensions [148]. There are, however, questions regarding the limits to which dimensions can be reduced. These pertain to phenomena associated with deepsubmicron dimensions and increased electric field strengths, such as mobility degradation [149], inversion-layer broadening [150], tunneling through the gate insulator, and the onset of velocity saturation, as well as such practical difficulties as linewidth and overlay control, thin insulator reliability, shallow-junction fabrication, and limitations of contact and spreading resistivities. On the other hand, there may be advantageous effects awaiting as well, such as the possibility of velocity overshoot [151] in very short devices and the weakening of detrimental effects associated with energy thresholds such as avalanche breakdown and hotcarrier injection into insulators. While there is a substantial amount of theoretical work addressing the perceived limits of scaling, very little experimental work exists in the sub-0.5- μ m regime. A project was therefore initiated 1) to study scaling MOSFETs down to the 0.1-µm level; 2) to fabricate test vehicles in as conventional a manner as possible which can then serve as a reference point for radical departures in processes and/or device concepts; 3) to see what transconductance and switching times are achievable in such a technology; and 4) to investigate what, if any, novel effects are observed at these dimensions.

A variety of different structures were assembled in seven different chip designs for this investigation. They range from parametric test sites such as capacitors, linewidth, overlay and bias monitors, to single devices and simple circuits such as inverter chains and ring oscillators. On the seven chips, most of the structures were repeated with identical dimensions except for the gate length, which was varied from $0.07~\mu m$ to $0.25~\mu m$. NMOS devices designed for LN₂ operation were the first goal [152]. Figure 9 is a schematic cross section of the basic device along with key design and process features; Figure 10 is a photomicrograph of a chip containing inverter chains with four different gate lengths.



Photomicrograph of a chip containing inverter chains and support circuits. The high-resolution area measures $0.25\times0.25~\text{mm}^2.$



BOTTO E

Summary of the gate-fabrication process (implants not shown).

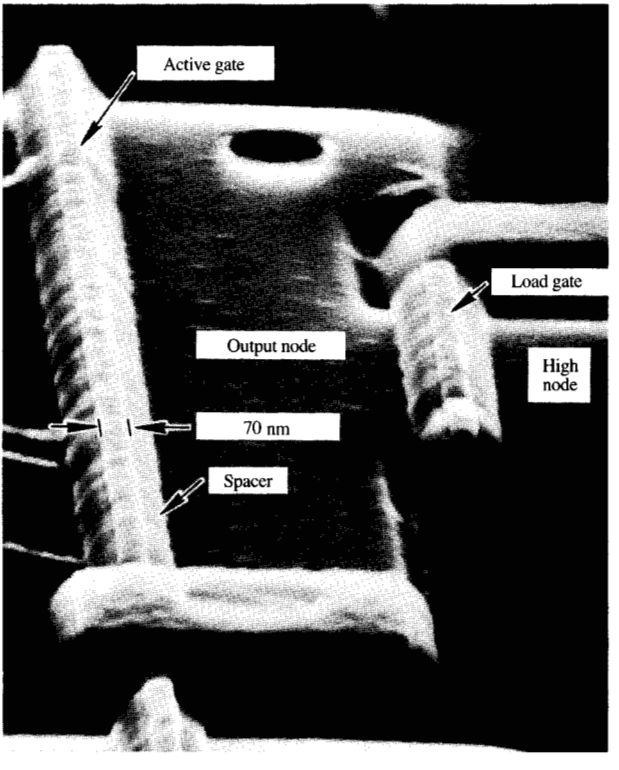


Figure 12

Scanning electron micrograph of an inverter after stripping the metal and conformal oxide. Diffusion and field regions and marks due to contact holes and nitride sidewalls are visible, together with 70-nm gates.

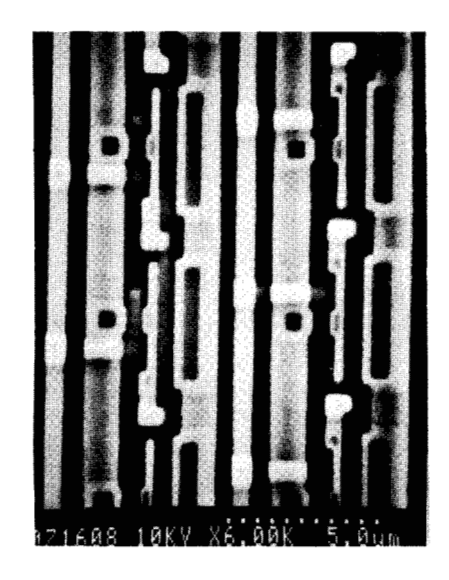


Figure 13

Section of a ring-oscillator indicating a contact and metal geometry which takes full advantage of the sub-30-nm overlay capability of e-beam fabrication.

Lithographic capability is clearly an important issue in this work. Not only is high resolution required for fabrication of the short gates, but equally important is the need to reduce parasitic effects caused by source and drain resistance and capacitance. Besides the use of low-resistance materials such as silicides, miniaturization of all device elements, and in particular, reduction of the distance between source/drain contacts and optimization of the contact size and geometry are key factors. Increased demands on level-to-level overlay and dimensional control in the contact process are the direct consequences.

All levels have been patterned by direct electron-beam writing using VS-6 [76]. Including the alignment marks with 0.25-um features, there were five levels in the process. The most critical step in terms of resolution was the fabrication of the gate level. Metal lift-off using double-layer PMMA resist was performed successfully for the complex gate pattern, which was used as an RIE mask to define the polysilicon gate structures. This process is summarized in Figure 11. Figure 12 shows 70-nm gates in a section of an inverter chain. Better than 30-nm alignment accuracy was achieved for level-to-level overlay, using tantalum-silicide marks with 0.25- μ m features. This was particularly important for the contact-gate-level overlay so that relatively large contact areas could be used, thus reducing the detrimental contact resistances. This can be seen in Figure 13, which shows a section of a completed ring-oscillator.

Details of the electrical design and of the processing have been described elsewhere [9, 153]. So far, approximately 75% of the tested structures have been operational. This includes some sites that depend on the operation of many devices, such as inverter chains. Figure 14 shows the drain characteristics of a series of devices with gate lengths of 0.2 μ m, 0.16 μ m and 0.1 μ m. One can see that the device characteristics in this scaled-down voltage regime appear almost "long-channel-like," with low output conductance. There is a clear trend toward improved performance with decreasing gate length both at room temperature (left column) and at 77 K (right column). A systematic decrease in switching time with decreasing gate length is observed, reaching a delay per gate of 13.1 ps for 0.1-\mu m devices at 77 K [154], which represents the fastest switching speed ever reported for silicon devices.

Figure 15 shows the characteristics of a 0.1- μ m device and a 0.07- μ m device at low temperature. The transconductances achieved here are 763 mS/mm and 912 mS/mm, respectively. These values are significantly higher than anything achieved to date in Si-FETs and are about equal to the best values with GaAs-MODFETs [155]. As will be discussed in more detail in a separate paper [156], these transconductance values, which have not been corrected for parasitic effects, are only possible if the electrons have significantly higher velocities in parts of the channel than the 1.1×10^7 cm/s which is considered the saturation velocity in

bulk silicon. As such, these devices exhibit significant velocity overshoot [157, 158].

Quantum structures and devices in metals and semiconductors

Aharonov-Bohm-effect studies

For Aharonov-Bohm studies, one critical dimension is the perimeter of the ring structures, which should be less than the inelastic scattering length. The ratio of the linewidth to the ring diameter is another important factor that has to be considered in the design of Aharonov-Bohm structures. The field enclosed by the ring produces periodic oscillations in the resistance, while the field piercing the wires produces aperiodic fluctuations. The characteristic field scales for the two effects are determined by the areas of the hole and the wires.

Investigations of the impact of a magnetic vector potential \hat{A} on the phase of the electron wave function (Aharonov– Bohm effect) have been conducted in a number of experiments with electrons in vacuum (e.g., [159]) and in superconductors (e.g., [160]). In normal metals [161], the initial work on the Aharonov-Bohm effect was accomplished using an SEM and contamination resist lithography. In Aharonov-Bohm experiments, the path of electrons is commonly split into two branches and then recombined. thus forming a closed-loop structure. If coherence is maintained between the two paths, interference effects can be observed. The magnetic flux enclosed by the loop shifts the relative phase of the partial waves according to $\Delta \Phi = e/\hbar \int \vec{A} \cdot ds$. A phase shift of 2π is achieved by an enclosed flux of h/e (or h/2e for superconductors). In metal loops, this phase shift results in conductance fluctuations of the device. The electron-beam nanolithography system VS-6 proved useful in generating large numbers of loops in various configurations, leading to a clear experimental separation of the normal h/e Aharonov–Bohm effect and h/2e oscillations [162].

The impact of electrostatic potentials on the phase of the wave function (electrostatic Aharonov–Bohm effect) had until recently been studied only with electrons in vacuum [163]. An electrical potential contributes to the fourth term of the four-vector product $A_{\mu}dx^{\mu}$. This term contains the scalar potential V associated with electric fields and time. The effect of the electrostatic potential is to cause a phase shift in the wave function of $\Delta \Phi = e/h \int V dt$. A potential difference between the two paths causes the partial waves following those two paths to arrive at the recombination point with relative phase shift.

In order to investigate the effect of electric fields on the phase of electrons in metal, a test structure was fabricated as shown in **Figure 16**. It consists of a closed square loop with dimensions of $0.8~\mu m$ by $0.8~\mu m$ and a linewidth of 70~nm. Two additional electrodes, each measuring $0.8~\mu m$ long and

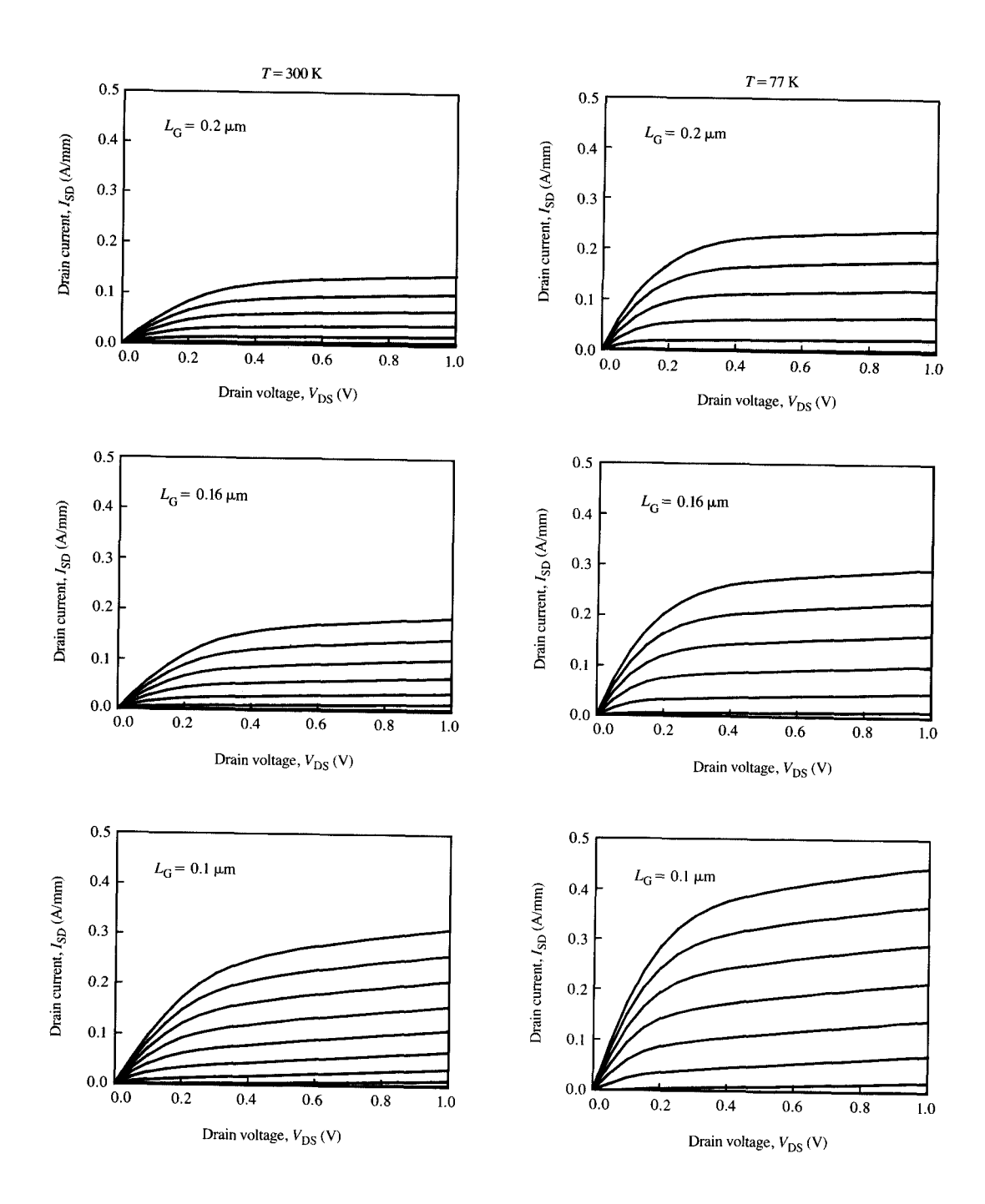
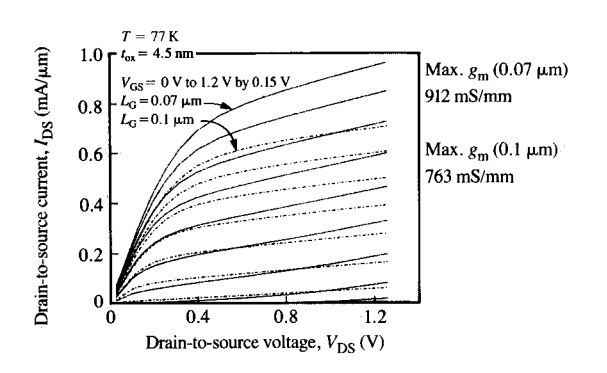
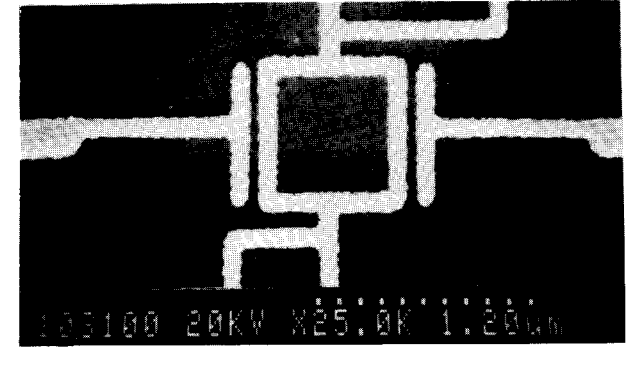


Figure 14

Measured FET characteristics for devices with 0.2- μ m, 0.16- μ m, and 0.1- μ m gate lengths at room temperature (left) and at liquid nitrogen temperature (right). The gate voltage was varied in each case from 0 V to 0.8 V in 0.1-V steps.

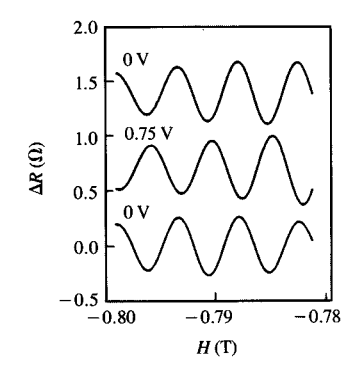




FET characteristics for a 0.1- μ m and a 0.07- μ m-gate-length device at liquid nitrogen temperature, exhibiting record transconductance.

Figure 16

Micrograph of test structure used for investigation of the electrostatic Aharonov–Bohm effect.



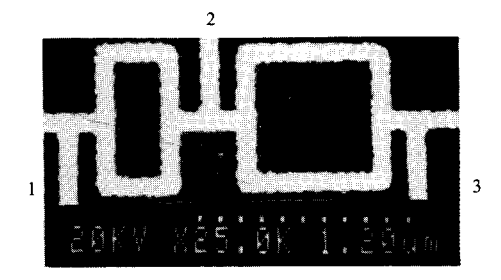


Figure 17

Electrostatically induced phase shifts of h/e oscillation.

Figure 18

Micrograph of test structure for study of nonlocal character of carrier wave function.

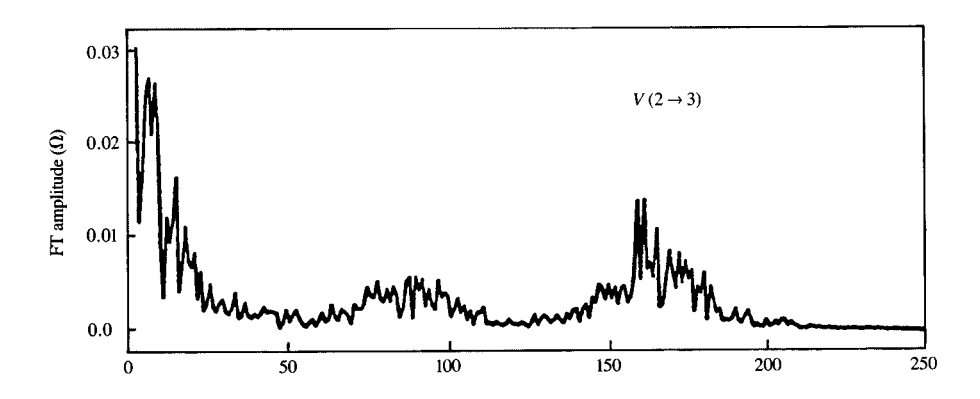
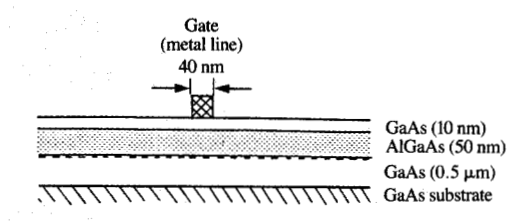
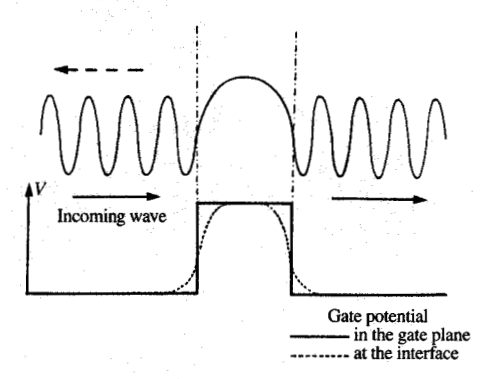


Figure 19

 $Spectrum\ of\ voltage\ fluctuations\ measured\ between\ terminals\ 2\ and\ 3\ of\ the\ structure\ in\ Figure\ 18.$





Cross section of a test structure for resonant scattering studies in a GaAs/AlGaAs transistor (top) and expected scattering behavior of an electron wave at a potential barrier (bottom).

70 nm wide, are introduced at close proximity (\approx 50 nm) to the two opposite legs of the loop. Voltages of opposite polarities can be applied to these electrodes to introduce the electrostatic effects. In addition, a magnetic field can also be applied normal to the loop to produce magnetically induced conductance fluctuations (h/e oscillations). This structure is fabricated on a plain silicon substrate by electron-beam lithography at 50 kV. The exposure was done in double-layer PMMA resist [12] with a total thickness of about 160 nm, followed by a lift-off of 60-nm-thick Sb.

Experiments have been carried out with this test structure by applying both a magnetic and an electric field at different combinations of intensities [164]. In the absence of the electric field, the well-established h/e oscillation of conductance is observed as shown in Figure 17 when the external magnetic field is increased. With the application of the electric field, a phase shift of the h/e oscillation was observed which increases with increasing electric field. It can be seen in Figure 17 that a phase shift of π was obtained with a voltage difference of ~ 0.75 V applied at the two electrodes. Removing the electric field causes the phase to revert to the initial position.

A structure consisting of two Sb loops in series, with a linewidth of 70 nm and a size of 0.4 μ m by 0.8 μ m and 0.8

 μ m by 0.8 μ m, respectively, connected by a 0.3- μ m-long wire (Figure 18), was used to investigate the nonlocal character of the carrier wave functions. The Aharonov-Bohm effect in one loop causes fluctuations of the voltage measured across the other loop. Figure 19 shows the fluctuation spectrum of the voltage measured across the larger loop with a characteristic peak at 160 tesla⁻¹. The peak at 80 tesla⁻¹ is due to the smaller loop (with half the area), which in the classical sense should not affect this measurement. More details can be found in [164–166].

Transmission resonances in GaAs/AlGaAs FET GaAs/AlGaAs heterostructures are well suited for quantum transport studies because the electrons at the interface of the two materials provide a large Fermi wavelength and elastic and inelastic scattering lengths. In the experiment described here, the effect of very narrow potential barriers on the transport in short one-dimensional GaAs/AlGaAs wires has been studied [167].

The top of Figure 20 shows a schematic cross section of the structure consisting of a very narrow gate electrode about 40 nm in width across a nominally 2-μm-wide and 10-μmlong channel of a GaAs/AlGaAs heterostructure. By applying a voltage to the gate electrode, a potential barrier can be introduced to the heterostructure to modulate the current flowing at the interface. The lower diagram in Figure 20 depicts the behavior of an incoming wave scattered at an ideal rectangular potential barrier created by the gate electrode: Resonance effects can be observed in those cases when the wavelength fits within the geometry of the potential barrier. Figure 21 shows a full view of a finished device with an enlargement of the 40-nm gate in the inset. The four bright gold pads at the two ends serve as the terminals for the four-point measurements between source and drain, while the fifth electrode in the center is for the connection to the gate. The fabrication procedures, all based on electron-beam lithography, are briefly summarized as follows:

- Formation of the contact pads using terpolymer/PMMA double-layer resist and lift-off of the ohmic contact material stack. The contact to the interface underneath is achieved by thermal diffusion.
- 2. Formation of the conduction channels by ion implantation to confine the conduction to only a narrow channel of 1-μm or 2-μm width between the source and drain and to the connecting paths to the two other test pads. This is achieved using a double-layer resist consisting of 140-nm siloxane over a 500-nm-thick polyimide. The exposed and developed siloxane negative resist is used as a mask for an oxygen dry-etch process of the polyimide, which is then used to mask the implantation. These nonimplanted areas can be recognized as slightly darker regions in Figure 21.

 Formation of the gate. This is a critical step performed using 120-nm-thick PMMA resist to lift off a 40-nm-wide AuPd electrode a few μm long and 40 nm thick.

Figure 22 shows the conductance-versus-gate-voltage characteristic of one of the fabricated devices. The transmittance of electron waves through a rectangular potential barrier is shown [Curve (a)] for comparison with the observed oscillatory fluctuations of conductance with gate voltage [Curve (b)]. Some correlation of the oscillation peaks of these two curves can be seen, which may be interpreted as evidence of the expected resonance effects. However, this observation is inconclusive, since the gate potential within the GaAs/AlGaAs interface is expected to be a smooth continuous profile rather than the idealized rectangular barrier indicated in the lower portion of Figure 20. Simulations with a smoothed potential show a conductance versus gate voltage in which the amplitude of the resonance peaks is highly smeared out in comparison with a simple rectangular well [168]. A more detailed analysis of the results and contributing factors can be found in [167].

One-dimensional and zero-dimensional electron systems in GaAs/AlGaAs heterostructures

One- and zero-dimensional electron systems defined by finepitch gratings and very small dots were fabricated in GaAs/ AlGaAs heterostructures [169, 170]. The starting material consisted of an MBE-grown modulation-doped heterostructure with two unique features: a thick GaAs cap layer and a heavily doped GaAs substrate, which facilitate capacitance measurements of the density of states. An outline of the fabrication procedure is shown schematically in Figure 23. High-resolution electron-beam lithography was used to pattern grating and dot etch masks consisting of PMMA resist (grating) or NiCr/Au (dots) with widths ranging from 100 nm to 400 nm. The patterns were then transferred into the heterostructures by etching through these masks. Selective GaAs/AlGaAs reactive ion etching using freon12/helium [171] was employed. This enabled precise etching of the top GaAs capping layer in order to deplete the two-dimensional electron gas beneath the etched surface. Gates (200 \times 200- μ m squares) comprising 300 nm of Ni/Au were defined optically on the lines or dots. Figure 24 shows scanning electron micrographs of the grating and dot structures. Because many lines (250-500) or dots (160 000-1 000 000) were measured in parallel, good uniformity in the dimensions of the structures was crucial, since dimensional variations would tend to diminish or obliterate the one- and zero-dimensional effects. Oscillations in capacitance spectroscopy reflecting discrete energy levels associated with one- and zero-dimensional electronic systems were observed [Figures 25(a) and (b)]. The experimental results were in accord with theoretical predictions [169]. This research

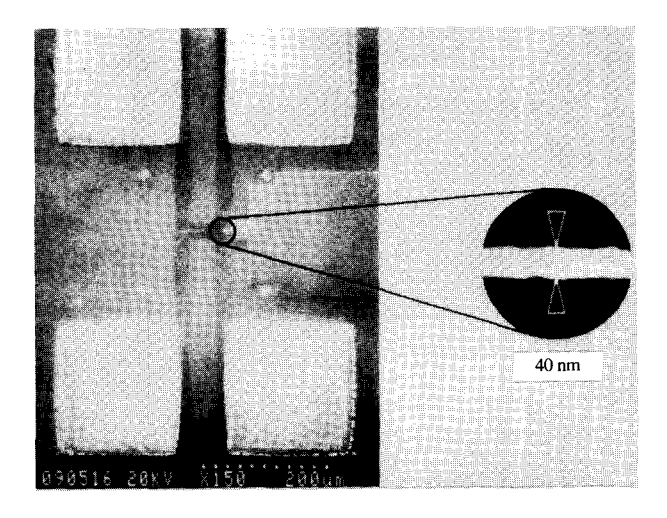


Figure 21

Micrograph of finished test transistor, showing 40-nm gate.

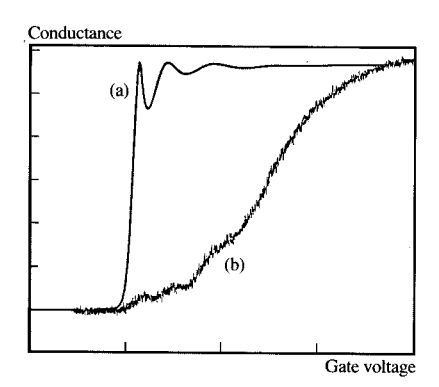
demonstrated the first clear and direct observations of zeroand one-dimensional states, and the high-precision lithographic capability of the VS-6 electron-beam writing system.

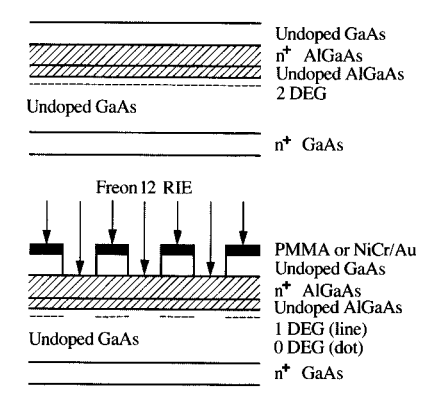
• Cryogenic tunneling devices

Superconductor–semiconductor–superconductor weak links have received increased attention in recent years for their possible applications to three-terminal (FET-like) superconducting devices and in the study of the physics of the superconductor/semiconductor interface [172–175]. The basic configuration of this type of weak link consists of two superconducting electrodes separated by a narrow gap of normal semiconductor material. When the gap is made sufficiently small, in the range of a fraction of a micron up to a few microns, the proximity effect of the superconducting electrodes can result in the transfer of Cooper pairs through the semiconductor.

Weak-link structures were fabricated using InAs as the semiconductor, as shown in **Figure 26**. The InAs is grown on semi-insulating GaAs as a continuous thin film, and the device isolation is then achieved by mesa etching. The superconducting pads (Nb) and the gap are defined by electron-beam lithography using double-layer PMMA resist (200 nm thick) and lift-off. The gap width fabricated varied between 0.1 and 2 μ m, and proximity-effect corrections were applied to the electron-beam exposures to achieve accurate control of the gap width. I/V characteristics of a number of devices with different gap widths were measured at liquid helium temperature.

Figure 27 shows a micrograph of a finished weak-link device based on Nb-InAs-Nb. The gap width between the

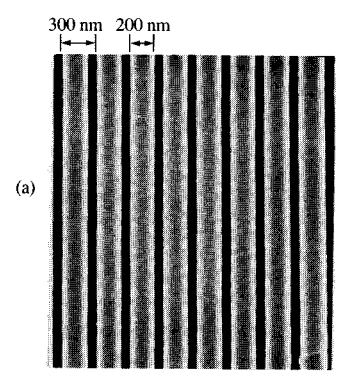




Conductance vs. gate voltage of a resonant scattering device: (a) expected behavior for rectangular barrier; (b) experimental result.



Fabrication of grating and dot structures.



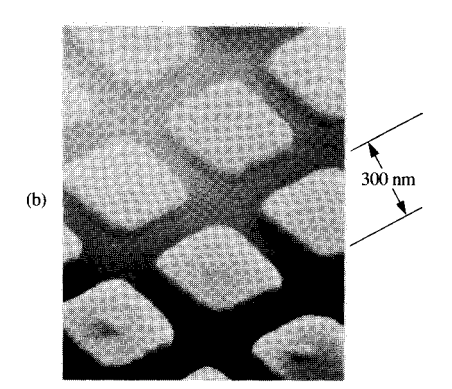
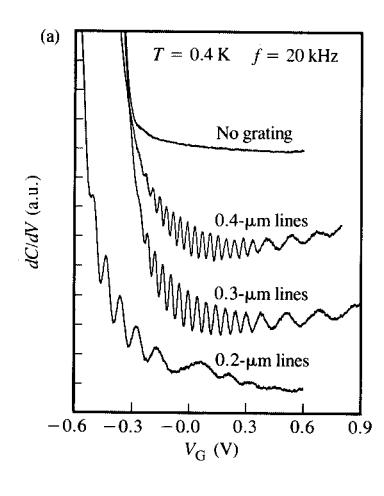
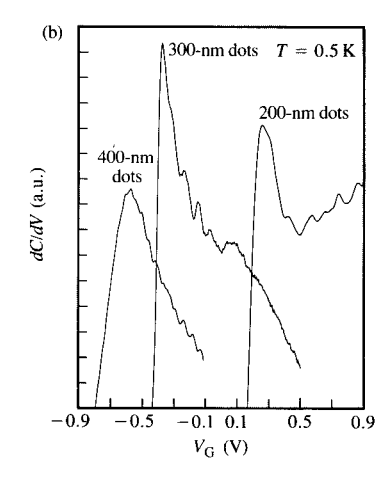


Figure 24

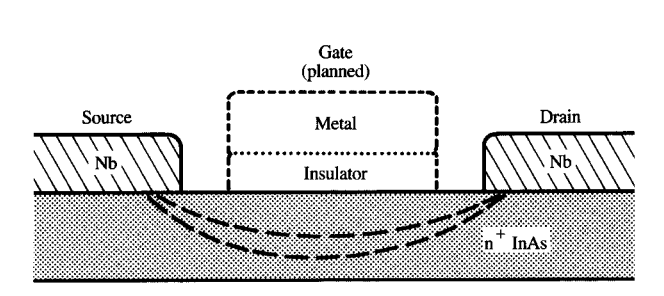
Scanning electron micrographs: (a) grating with 200-nm linewidth and 300-nm pitch; (b) 300-nm-wide dots with 500-nm period.





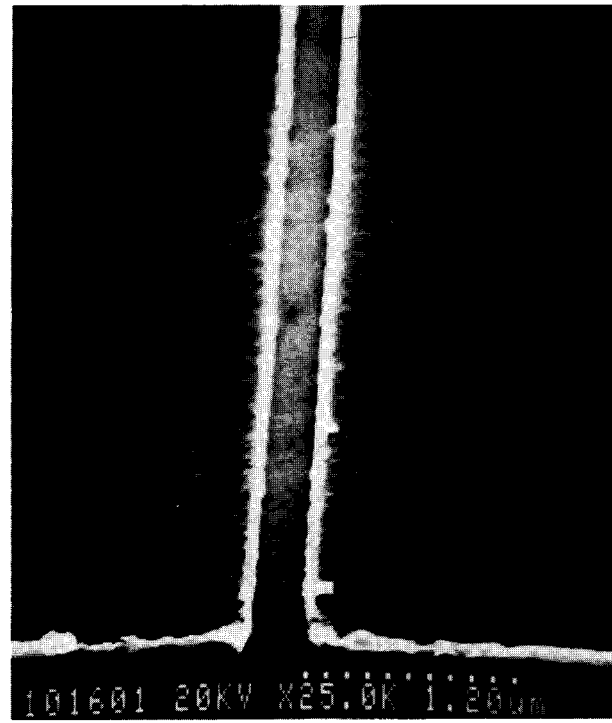
Elatina 25

Capacitance spectroscopy of (a) one-dimensional (lines) and (b) zero-dimensional (dots) electron systems.



Undoped GaAs buffer layer



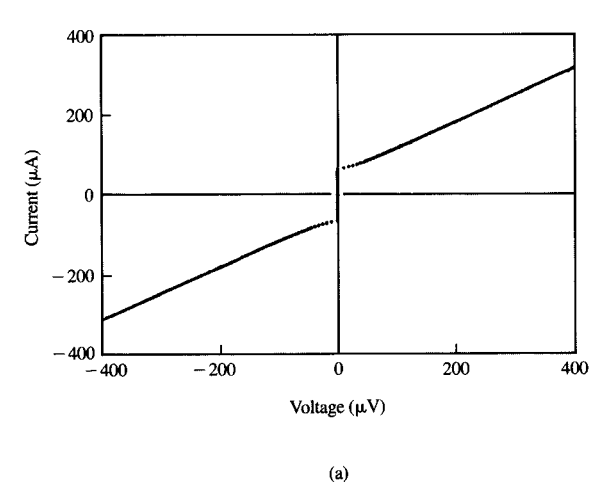


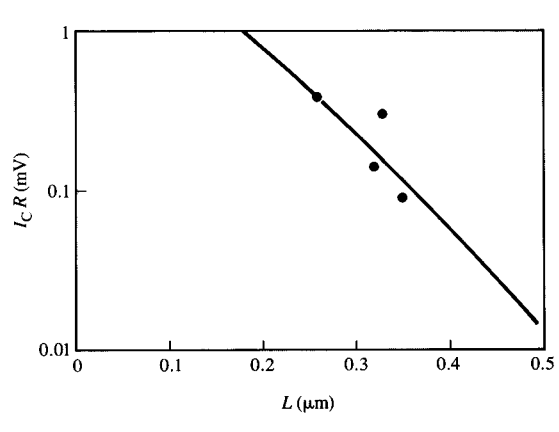
Entere 26

Schematic cross section of an InAs-coupled weak link.

Figure 27

Scanning electron micrograph of a finished weak link.





(b)

Emme 28

Current-voltage characteristic for an InAs-coupled Nb weak link (a), and the $I_{\rm C}R$ product at 4.2 K vs. measured gap width (b). The solid curve is the prediction of Likharev's model.

Section of an array of Permalloy particles nominally 0.1 μm by 0.3 μm in size, 0.5 μm by 0.6 μm apart.

Nb electrodes (the edges of which are the vertical bright areas) is $0.25 \mu m$. Figure 28(a) shows a typical current-voltage characteristic of such a weak link; the superconducting current across the gap is clearly visible. Figure 28(b) shows the variation of the critical current-resistance product I_cR versus the gap width, together with the theoretical values based on Likharev's model [176] (for experimental details see Kleinsasser et al. [175]).

◆ Arrays of submicron particles

Particles 100 nm or less in size are known to have properties different from those of larger particles of the same materials or even bulk material. They are used as catalysts and in filters, magnetic media, and new materials. Arrays of small particles with controlled size and distances bring another degree of freedom which can influence their properties, namely the particle interaction. New material properties can be expected if, for example, films are grown by nucleation from well-defined and well-spaced nucleation centers. One particular field of interest which is described in more detail has to do with the behavior of arrays of magnetic particles.

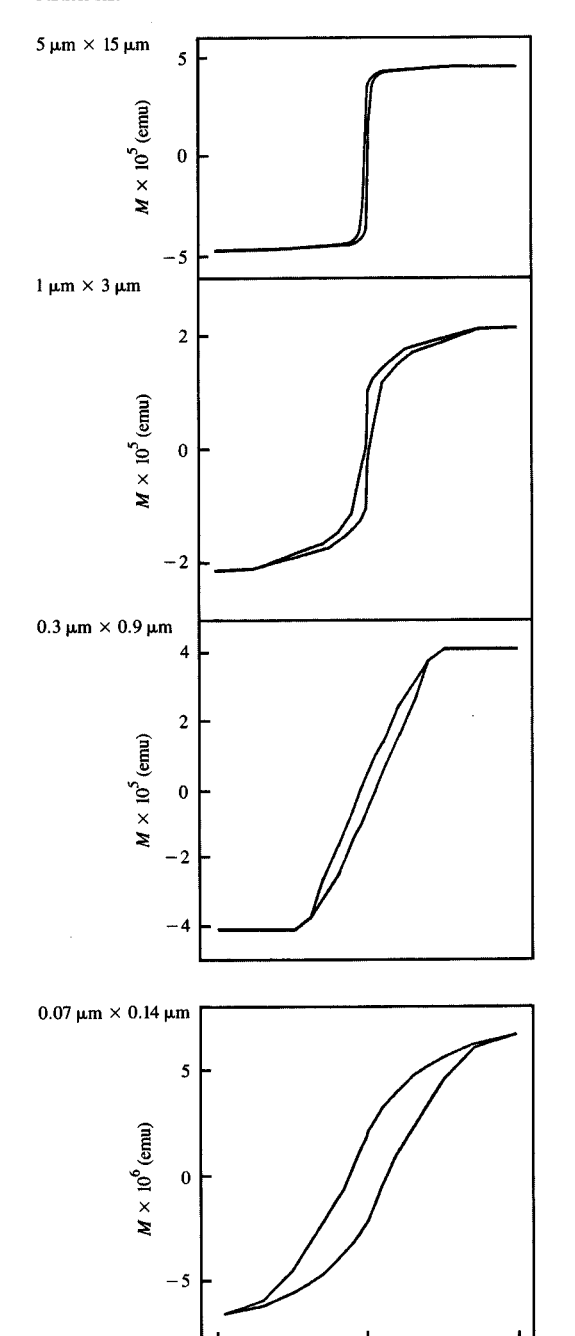
Arrays of submicron Permalloy particles

An accurate description of the magnetic properties of strongly interacting magnetic particles remains an unsolved problem. For numerical simulations the knowledge of the microscopic status of an interacting spin system would be desirable. This requires knowledge (and control) of the particles' size, shape, morphology, magnetic properties, and their relative orientation and spacing. With that in mind, controlled arrays of Permalloy particles were prepared as part of a program to determine the magnetic properties of verifiable single-domain particles and the effects of interactions between them. The particle arrays were made using high-resolution electron-beam lithography in doublelayer PMMA, evaporation of Permalloy from a single source whose composition had been adjusted to account for the different vapor pressure of Ni and Fe, and lift-off. The particle sizes and spacings vary from 5- μ m by 15- μ m particles with 25- μ m spacing to 0.07- μ m by 0.1- μ m particles with 0.25- μ m spacing. Each array consists of 10^6 and 10^7 identical particles with identical spacing.

Figure 29 shows a section of such an array with particles nominally 0.1 μ m by 0.3 μ m in size, 0.5 μ m by 0.6 μ m apart. Magnetization measurements were done using a SQUID magnetometer. Figure 30 shows a series of hysteresis loops for arrays with large interparticle spacings and varying particle size. The hysteresis loop at the top for 5- μ m by 15- μ m particles has H_c of ~6 Oe, which is still comparable to that of films as deposited (~2 Oe). As the particle size becomes smaller, H_c increases to a value of $H_c = 120$ Oe for the 0.07- μ m by 0.14- μ m particles, although the shape of the loops indicates that even the smallest particles are not single domains. Figure 31 shows a series of hysteresis loops for identical particles but decreasing particle spacing from top to bottom. While H_c decreases with decreasing interparticle spacing, there are also unexpected changes in the general shape of the hysteresis loops [177]. (This work was performed in collaboration with S. Schultz and J. Smyth of the Center for Magnetic Recording Research, University of California at San Diego.)

◆ High-resolution Fresnel zone plate lenses for soft X-rays
The successful development of nanostructure fabrication
techniques, particularly electron-beam lithography, created
a favorable situation for the fabrication of high-resolution
X-ray optical devices [178–181]. Especially interesting are
Fresnel zone plates acting as X-ray lenses [180–185]. When
performed with suitable lenses, soft X-ray microscopy, a
quickly evolving and promising research technique, offers
resolution achieved only by electron microscopy and has
special advantages for the investigation of thick, unstained,
wet and live biological specimens [115, 185–188]. In
material analysis it opens new possibilities such as elemental
mapping and spatially resolved photo-electron spectroscopy
with substantially higher resolution than that currently

Particle size



Particle spacing

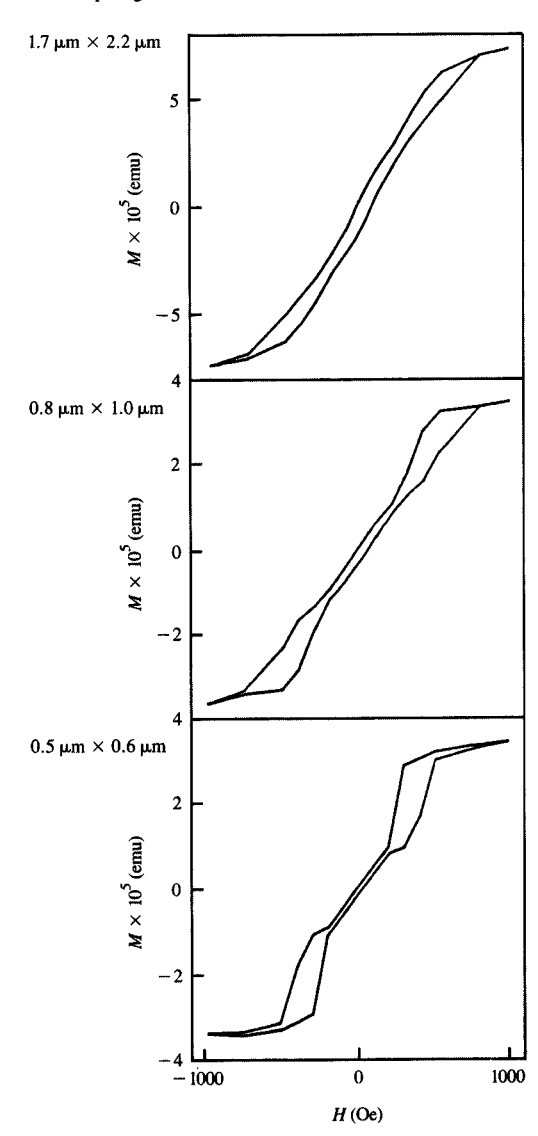


Figure 30

Hysteresis loops for series of arrays with large interparticle spacing and varying particle size.

0

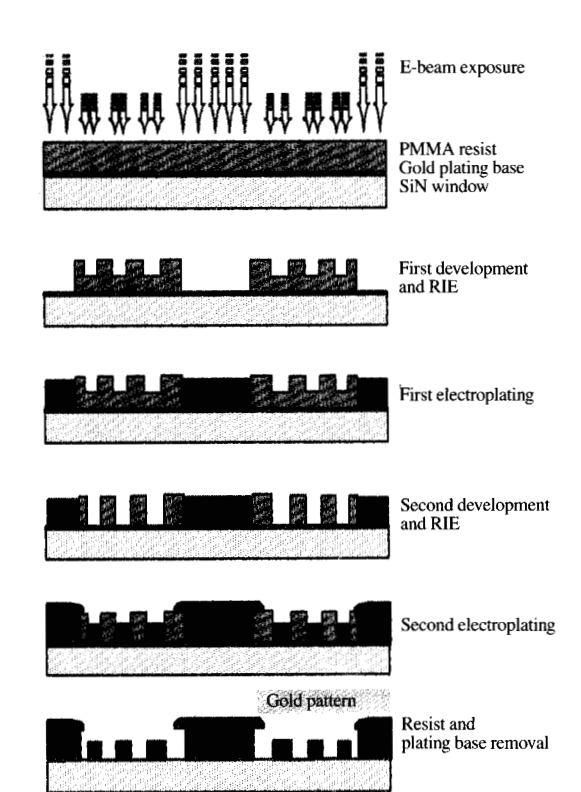
H (Oe)

1000

Figure 3

Hysteresis loops for series of arrays of identical particles but decreasing particle spacing from top to bottom.

- 1000



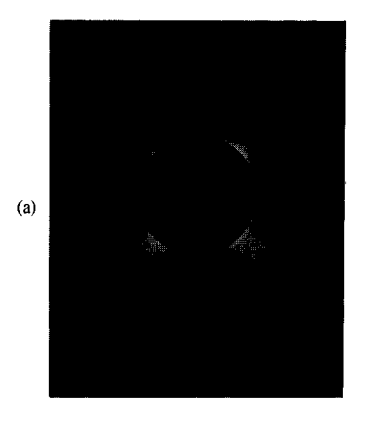
Single-exposure double-development/double-plating process for zone-plate fabrication.

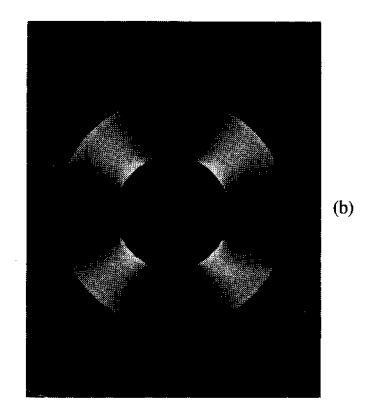
available [189]. Fresnel zone plates of a focal length f at a wavelength λ consist of N alternating opaque and open rings with the radii $R_n \simeq \sqrt{nf\lambda}$, $n=1,2,\cdots,N$. The diffraction-limited resolution δ is roughly equal to the width Δr of the outermost zone: $\delta \sim \Delta r = \sqrt{f\lambda} / 2\sqrt{N}$, and can be achieved if random displacement of the zones is less than one third of that value. Thus, the zone plate performance depends on the capability of high-resolution fabrication with an accuracy of the order of 16 nm for the 50-nm zone plates. A scanning X-ray microscope requires zone plates with a thick central stop and an outer rim [115].

The zone plates were fabricated by electron-beam lithography using a single-exposure double-development/double-plating technique [185], as shown in Figure 32. PMMA resist 180–200 nm thick was spun on a \approx 30-nm-thick gold electroplating base evaporated on the 100-nm-thick silicon nitride membrane. A novel method for monitoring the resist development of the fine features was used [185]. This utilized form birefringence caused by the

arrangements of the submicron discontinuities on the substrate surface. In the optical microscope with polarized light and crossed analyzer, a distinct change of the reflected intensity is observed during the final stages of the development. Figure 33 shows a zone-plate pattern with 70nm features in cross-polarized light: (a) shortly before and (b) after the completion of development. A highly reflective substrate increases the effect. This method proved to be useful for features down to 30 nm (possibly to ~4 nm). For characterization of the zone shape, the moiré pattern technique was used. The superposition of two images of an elliptical zone plate rotated 90° relative to each other produces a very distinctive pattern [185]. Figure 34 shows moiré patterns of an elliptical zone plate with $\Delta R/R = 0.7\%$. The micrographs were obtained in a scanning electron microscope by a double exposure with rotation and shift of the plate. Calibration of field size and orthogonality allows fabrication of zone plates with negligible ellipticity. The efficiency [115, 185] of the zone plates was determined as the ratio of the flux concentrated in the focus to the incident flux. The resolution [115, 185] was measured using a knifeedge technique and defined as the distance between the intensity change from 75% to 25%. Figure 35 shows a nominal resolution of 75 nm for a 50-nm lens using this technique.

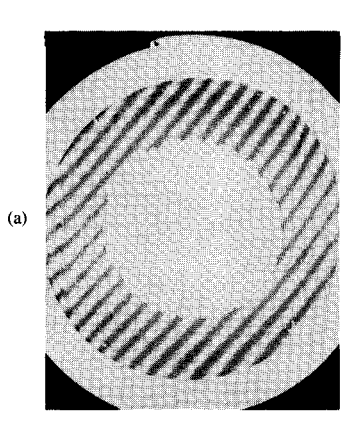
Three series of zone plates have been fabricated with outer zone width of 100 nm (149 zones), 70 nm (205 zones), and 50 nm (311 zones) [185]. They are designed with focal lengths of 2.0 mm, 1.3 mm, and 1.0 mm, respectively, for 3.1-3.2-nm wavelength. All zone plates have an outer diameter $\sim 60 \,\mu\text{m}$ and the central stop diameter $\sim 30 \,\mu\text{m}$. The 100-nm lenses demonstrated the highest efficiency, i.e., 4.6% to 5.2%, in contrast to the calculated value of 6.4% based upon a 140-nm/60-nm = 2.33 opaque-to-open-ringwidth ratio. The 70-nm plates have an outer diameter of 57 um and a 500-nm-thick 28-um-diameter central stop (Figure 36). The zones are 110 nm thick and the opaque/open ratio is 90 nm/50 nm. In the tests this lens achieved a spatial resolution of 95 nm and a diffraction efficiency of 2.9%. The 50-nm plates have a 600-nm-thick central stop and 100-nmthick zones with a 70-nm/30-nm opaque/open ratio, as shown in Figure 37. A resolution of 75 nm and 1.3% efficiency characterize this lens. The measured and calculated values of the ring widths, absorber thickness, efficiency, and resolution for the fabricated zone plates are summarized in Table 4. Considering the uncertainty in the knife-edge quality, the values obtained for the resolution are consistent with the near-diffraction-limited performance. The zone plates have been successfully used at the Brookhaven National Laboratory in a scanning X-ray microscope. X-ray images of biological specimens and artificial structures were formed at $\lambda = 3.2$ nm with the resolution in the 70-100-nm range [115, 185]. A highresolution X-ray image of a subcellular vesicle in a freshly

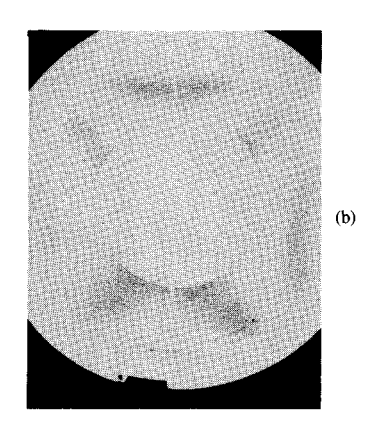




E ITTITE KK

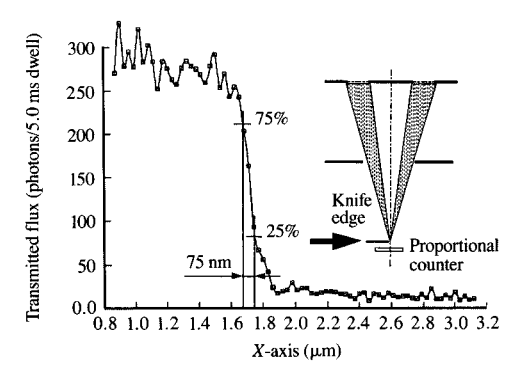
Zone-plate pattern with 70-nm features viewed in optical microscope with cross-polarized light at two development stages: (a) underdeveloped; (b) fully developed.





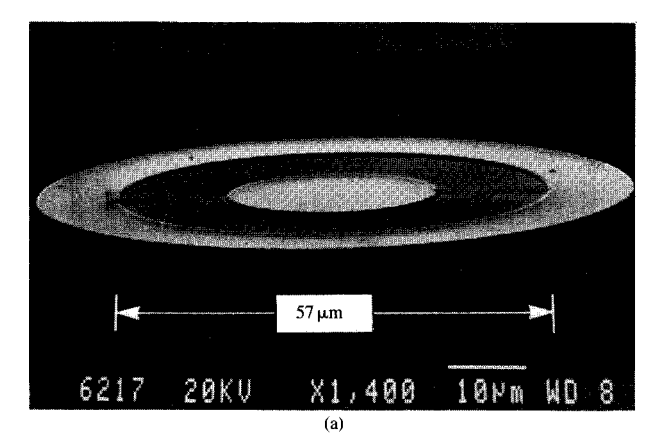
Entra Contract

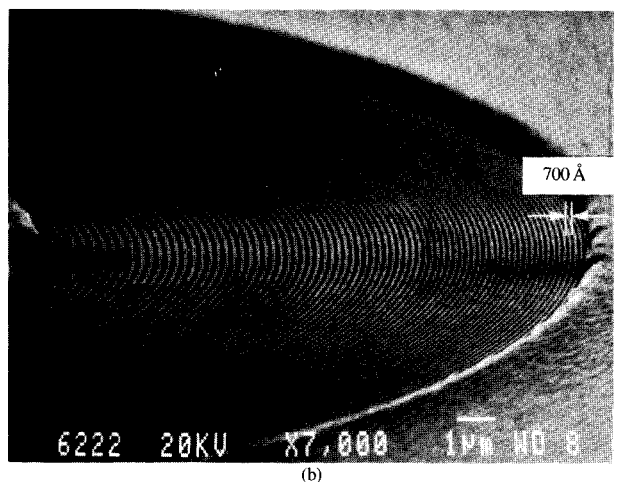
Moiré patterns observed using double SEM exposure of a slightly elliptical 100-nm zone plate with relative difference in radii $\Delta R/R = 0.7\%$: (a) 180° rotation with a shift of the zone plate between the exposures; (b) 90° rotation of the zone plate between exposures.



Entite S

Knife-edge measurements for a zone plate with 50-nm outermost zone width showing 75-nm nominal resolution.





Gold Fresnel zone plate with 70-nm nominal outer zone width: (a) full view; (b) area of working zones.

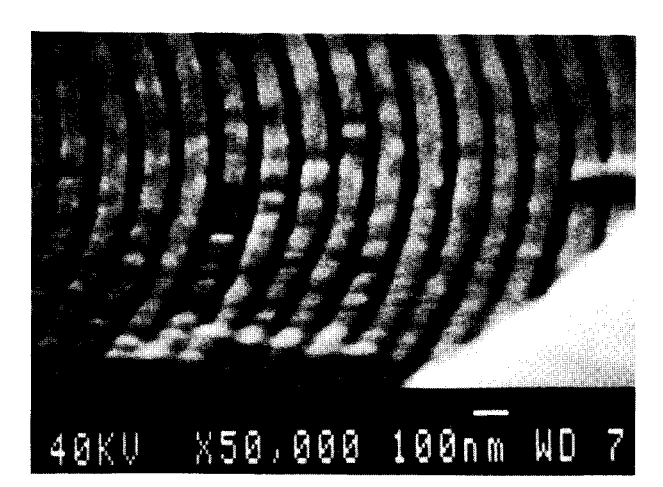


Figure 37

Gold Fresnel zone plate with 50-nm nominal outer zone width: close-up view of outer zones.

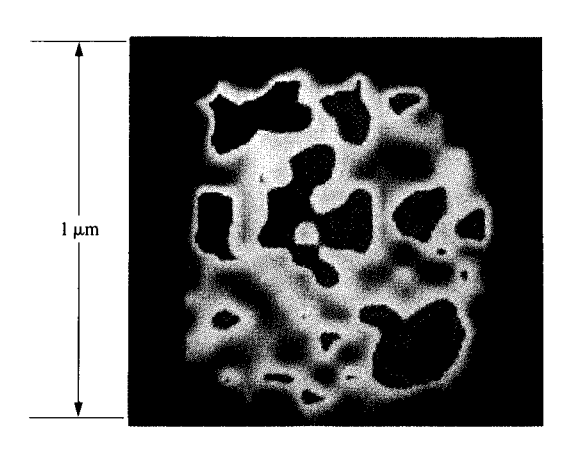


Figure 38

X-ray image of an unaltered 1-µm-diameter pancreatic secretion granule, obtained with the scanning X-ray microscope at a wavelength of 3.2 nm. The protein distribution in the granule corresponds to high absorption areas and is presented by blue (high carbon content) spots and areas within the image of the granule. The dark region around the granule is the aqueous environment. Fine details as small as 70 nm can be observed.

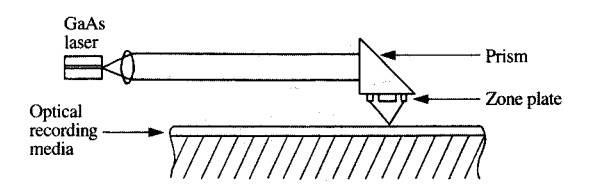


Figure 39

Illustration of use of zone-plate lens in optical recording head.

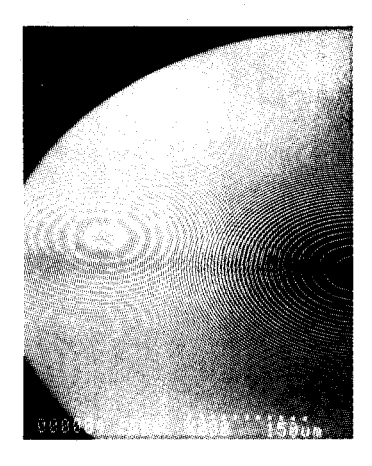


Figure 40

Scanning electron micrograph of a 900- μ m-diameter PRFZP with 0.88 μ m of PMMA on a quartz substrate, fabricated by electron-beam lithography: low-magnification overview.

prepared aqueous suspension of zymogen granules from the pancreas of a rat is shown in Figure 38. The image shows evidence of internal structure (not seen previously) with details to ~70 nm. (This work was performed in collaboration with H. Ade, J. Kirz, and I. McNulty, Department of Physics, SUNY Stony Brook, New York; H. Rarback and D. Shu, National Synchrotron Light Source, Brookhaven National Laboratory, New York; and D. Attwood, Center for X-ray Optics, Lawrence Berkeley Laboratory, University of California, Berkeley.)

• Zone plates for optical recording

The microfabrication of Fresnel zone plates has been studied by various groups for application in focusing X-ray optics, as described in the previous section. However, there are only a few examples for the microfabrication of Fresnel zone plates for application in optics [190-193]. Theoretically, blazed phase-reversal Fresnel zone plates (PRFZPs) or Kinoform lenses can have an efficiency approaching 100% [194], while at the same time providing a low-profile, lightweight optical focusing element. Such elements might be of interest in optical recording, as illustrated in Figure 39. The zone plates can be fabricated with high accuracy and flexibility using electron-beam lithography and microfabrication technology. For a good approximation of the surface profile of a Kinoform lens in an electron-sensitive resist layer, the exposure dose must be varied radially for rings with width of a fraction of the wavelength to obtain the desired relief structure after resist development. As an initial study, a series of unblazed phase-reversal Fresnel zone plates were fabricated on quartz substrate using PMMA as the phasereversal medium. An 856-nm-thick PMMA layer is required for a π phase shift at the wavelength of 830 nm of a GaAs laser, taking into account the refractive index of n = 1.485 of PMMA. The PMMA was exposed in the high-resolution electron-beam system VS-6 at 25 kV. PRFZPs for a resolution of 1-µm spot size with a numerical aperture of NA = 0.5 and diameters (also the focal lengths) of 250 μ m to 900 µm were made. A portion of a 900-µm-diameter PRFZP is shown in Figure 40. An initial optical characterization of the PRFZPs was carried out using the collimated light of a GaAs laser and a microscope with an infrared-sensitive SIT TV camera to measure focal lengths and focused spot diameter. Within the accuracy of this initial measuring setup, the results for focal length and spot size were in reasonable agreement with theoretical expectations [195].

Conclusion

The activities in nanostructure research are expected to increase rapidly for both technology and science applications. Semiconductor technology, especially silicon FET memory, is most demanding in lithography, and memory circuits with 250-nm feature size are projected for the next decade. The need to explore the sub-100-nm regime

Table 4 Comparison of measured and theoretical diffraction efficiencies and resolution for several zone plates.

Min. zone (nm)	Ring width (nm)		Thickness (nm)		Efficiency (%)		Resolution (nm)	
	opaque	open	zone	stop	exp.	calc.	exp.	calc
100	140	60	140	1000	5.2	6.4	130	110
70	95	45	110	500	2.9	5.7	95	70
50	70	30	100	600	1.3	5.2	75	52

is therefore both real and urgent. The results of the 0.1- μ m FETs discussed in this paper with transconductance of 912 mS/mm and switching speed of 13.1 ps are important for future enhancement of the FET silicon technology. In addition, radically new device concepts based on ultrasmall structures are beginning to emerge. In the physical sciences, structures with dimensions at the 10- to 100-nm scale have already enabled a number of fundamental studies to be conducted on effects dominated by quantum phenomena. The range of this research is expected to enter the sub-10-nm regime in the near future and may ultimately reach the molecular level. The scope may well expand from the field of physical science today to the fields of biological and medical sciences in the future.

Acknowledgments

The authors wish to acknowledge the technical contributions by many of their colleagues in the electron-beam-technology and resist-processing areas at the IBM Thomas J. Watson Research Center. Two visiting scientists, H. Schmid (now with Robert Bosch GmbH, Reutlingen, FRG) and H. Koops (now with the University of Darmstadt, FRG) are also acknowledged. The work on the various nanostructure and device programs has been possible only through the collaboration of a number of participants, who have been acknowledged either directly in the text or by reference to their relevant publications.

References

- C. D. W. Wilkinson, "Fabrication of Very Small Structures," *Examining the Sub-Micron World*, R. Feder, J. McGowan, and D. M. Shinozaki, Eds., Plenum Press, New York, 1986, p. 215.
- S. Namba, "Research Project on Nanometer Structure Electronics," Microelectron. Eng. 2, 3 (1984).
- R. E. Howard, P. F. Liao, W. J. Skocpol, L. D. Jackel, and H. G. Craighead, "Microfabrication as a Scientific Tool," Science 221, 117 (1983).
- E. D. Wolf and J. M. Ballantyne, "Research and Resource at the National Submicron Facility," VLSI Electronics: Microstructure Science, N. G. Einspruch, Ed., Academic Press, Inc., New York, 1981, Vol. 1, p. 129.
- D. E. Prober, "Quantum Transport in Microstructures," Microelectron. Eng. 5, 203 (1986).
- R. B. Laibowitz, A. N. Broers, J. T. C. Yeh, and J. M. Viggiano, "Josephson Effect in Nb Nanobridges," Appl. Phys. Lett. 35, 891 (1979).

- G. J. Iafrate and K. Hess, "High Speed Transport in Ultrasmall Dimensions," VLSI Electronics: Microstructure Science, N. G. Einspruch, Ed., Academic Press, Inc., New York, 1985, Vol. 9, p. 207.
- H. Schmid, S. A. Rishton, D. P. Kern, S. Washburn, R. A. Webb, T. N. Jackson, A. Kleinsasser, T. H. P. Chang, and A. Fowler, "Fabrication of Quantum Devices in Metals and Semiconductors," J. Vac. Sci. Technol. B 6, 122 (1988).
- C. G. Smith, H. Ahmed, and M. N. Wybourne, "Fabrication and Phonon Transport Studies in Nanometer Scale Free-Standing Wires," *J. Vac. Sci. Technol. B* 5, 314 (1987).
 D. C. Flanders, "Nanometer Structure and Device
- D. C. Flanders, "Nanometer Structure and Device Fabrication," *Microelectron. Eng.* 2, 82 (1984).
- S. Mackie and S. P. Beaumont, "Materials and Processes for Nanometer Lithography," Solid State Technol. 28, 117 (August 1985).
- A. N. Broers, "High Resolution Lithography (Some Comments on Limits and Future Possibilities)," *The Physics and Fabrication of Microstructures and Microdevices*, M. J. Kelly and C. Weisbuch, Eds., Springer-Verlag, New York, 1986, p. 2.
- A. N. Broers, "Practical and Fundamental Aspects of Lithography," *Materials for Microlithography*, L. F. Thompson, C. G. Willson, and J. M. Frechet, ACS Symposium Series, American Chemical Society, Washington, DC, 1984, p. 11
- T. E. Everhart, "Fundamental Limits of Lithography," *Materials for Microlithography*, L. F. Thompson, C. G. Willson, and J. M. Frechet, ACS Symposium Series, American Chemical Society, Washington, DC, 1984, p. 5.
- R. E. Howard and D. E. Prober, "Nanometer-Scale Fabrication Techniques," VLSI Electronics: Microstructure Science, N. G. Einspruch, Ed., Academic Press, Inc., New York, 1982, Vol. 5, p. 146
- C. D. W. Wilkinson and S. P. Beaumont, "Electron Beam Nanolithography," The Physics and Fabrication of Microstructures and Microdevices, M. J. Kelly and C. Weisbuch, Eds., Springer-Verlag, New York, 1986, p. 36.
- D. P. Kern, P. J. Houzego, P. J. Coane, and T. H. P. Chang, "Practical Aspects of Microfabrication in the 100 nm Regime," J. Vac. Sci. Technol. B 1, 1096 (1983).
- A. N. Broers and T. H. P. Chang, "High Resolution Lithography for Microcircuits," *Microcircuit Engineering*, H. Ahmed and W. C. Nixon, Eds., Cambridge University Press, Cambridge, England, 1980, p. 1.
- F. Emoto, K. Gamo, S. Namba, N. Samoto, R. Shimizu, and N. Tamura, "Nanometer Structure Fabrication Attained by Nanometer E-Beam Lithography System (NSF-1)," Microelectron. Eng. 3, 17 (1985).
- H. Beneking, "A Field Emission E-beam System for Nanometer Lithography," Microelectron. Eng. 2, 74 (1984).
- M. Isaacson, A. Muray, M. Scheinfein, I. Adesida, and E. Kratschmer, "Nanostructure Fabrication Using Electron Beam Lithography," *Microelectron. Eng.* 2, 58 (1984).
- 23. R. E. Howard, H. G. Craighead, L. D. Jackel, and P. M. Mankiewich, "Electron Beam Lithography from 20 to 120 keV with a High Quality Beam," J. Vac. Sci. Technol. B 1, 1101 (1982)
- T. H. Newman, K. E. Williams, and R. F. W. Pease, "High Resolution Patterning System with a Single Bore Objective Lens," J. Vac. Sci. Technol. B 5, 88 (1987).
- G. A. Jones, S. Blythe, and H. Ahmed, "Very High Voltage (500 kV) Electron Beam Lithography for Thick Resists and High Resolution," J. Vac. Sci. Technol. B 1, 120 (1987).
- M. Hassel-Shearer, H. Takemura, M. Isobe, N. Goto, K. Tanaka, and S. Miyauchi, "Development of Nanometric Electron-Beam Lithography System (JBX-5DII)" J. Vac. Sci.

- Techol. B 4, 64 (1986).
- K. Iwadate, R. Yamaguchi, K. Hirata, and K. Harada, "A Novel High-Speed Nanometric Electron Beam Lithography System: EB-F," J. Vac. Sci. Technol. B 5, 75 (1987).
- N. Saitou, S. Hosoki, M. Okumura, T. Matsuzaka, G. Matsuoka, and M. Okyama, "Electron Optical Column for High Speed Nanometric Lithography," *Microelectron. Eng.* 5, 123 (1986).
- E. Kratschmer, D. Stephani, and H. Beneking, "High Resolution 100 keV E-Beam Lithography," *Microcirc. Eng.* 83, 3 (1983).
- P. J. Coane, D. P. Kern, A. J. Speth, and T. H. P. Chang, "An Electron Beam Microfabrication System for Lithography Below 1000 A," Proceedings of the 10th International Conference on Electron and Ion Beam Science and Technology, R. Bakish, Ed., Electrochemical Society, Pennington, NJ, 1982, p. 15.
- A. N. Broers, J. J. Cuomo, J. Harper, W. Molzen, R. B. Laibowitz, and M. Pomerantz, "High Resolution Electron Beam Fabrication Using STEM," 9th International Congress on Electron Microscopy, Toronto, 1978, p. 343.
- K. L. Lee and H. Ahmed, "An E-Beam Microfabrication System for Nanolithography," J. Vac. Sci. Technol. 19, 946 (1981).
- 33. H. G. Craighead and P. M. Mankiewich, "Ultra-Small Metal Particle Arrays Produced by High Resolution Electron-Beam Lithography," J. Appl. Phys. 53, 7186 (1982).
- I. A. Crutwell, W. V. Colbran, and B. A. Wallman, "E-Beam Tool Requirements for Nanolithography," SPIE (Society of Photo-Optical Instrumentation Engineers) Proc. 537, 2 (1985).
- A. N. Broers, "Electron and Ion Probes," Proceedings of the 5th International Conference on Electron and Ion Beam Science and Technology, R. Bakish, Ed., Electrochemical Society, Pennington, NJ, 1972, p. 3.
- 36. T. H. P. Chang, A. J. Speth, C. H. Ting, R. Viswanathan, M. Parikh, and E. Munro, "The Probe Forming and Deflection System for Vector Scan I E/B Lithography System," Proceedings of the 7th International Conference on Electron and Ion Beam Science and Technology, R. Bakish, Ed., Electrochemical Society, Pennington, NJ, 1976, p. 377.
- A. N. Broers, "Long Life LaB₆ Cathodes," J. Appl. Phys. 38, 1991 (1967).
- F. J. Hohn, T. H. P. Chang, A. N. Broers, G. S. Frankel, E. T. Peters, and D. W. Lee, "Fabrication and Testing of Single Crystal Lanthanum Hexaboride Rod Cathodes," J. Appl. Phys. 53, 1283 (1982).
- A. V. Crewe, D. N. Eggenberger, J. Wall, and L. M. Welter, "Scanning Electron Microscope: Is High Resolution Possible?" Science 154, 729 (1966).
- J. W. Butler, "Digital Computer Techniques in Electron Microscopy," Proceedings, 6th International Conference on Electron Microscopes, Tokyo, 1966, p. 119.
- L. Veneklasen, N. Yew, and J. Wiesner, "Application of Field Emission in High Current Electron Beam Lithography Optics," Proceedings of the 8th International Conference on Electron and Ion Beam Science and Technology, Electrochemical Society, Pennington, NJ, 1978, p. 880.
- L. W. Swanson and L. C. Crouser, "Angular Confinement of Field Electron and Ion Emission," J. Appl. Phys. 40, 4741 (1969).
- D. Tuggle, L. W. Swanson, and J. Orloff, "Application of a Thermal Field Emission Source for High Resolution High Current E-Beam Microprobes," J. Vac. Sci. Technol. 16, 1699 (1979).
- J. E. Wolfe, "Operational Experience with Zirconiated T-F Emitters," J. Vac. Sci. Technol. 16, 1704 (1979).
- N. Samoto, R. Shimizu, H. Hashimoto, N. Tamura, K. Gamo, and S. Namba, "A Stable High Brightness Electron Gun with Zr/W-Tip for Nanometer Lithography: I. Emission Properties in Schottky and Thermal Field-Emission Regions," *Jpn. J. Appl. Phys.* 24, 766 (1985).
- S. Hosoki, K. Takata, and H. Kaga, "Ti/W (100) Field Emission Source," Proceedings, Eleventh International

- Congress on Electron Microscopy, Kyoto, Japan, 1986.
- N. Saitou, S. Hosoki, M. Okumura, T. Matsuzaka, G. Matsuoka, and M. Okyama, "Electron Optical Column for High Speed Nanometric Lithography," *Microelectron. Eng.* 5, 123 (1986).
- M. G. R. Thompson, R. Liu, R. J. Collier, H. T. Carroll, E. T. Doherty, and R. G. Murray, "The EBES4 Electron Optical Column," J. Vac. Sci. Technol. B 5, 53 (1987).
- E. Munro, "Design and Optimization of Magnetic Lenses and Deflection Systems for Electron Beams," J. Vac. Sci. Techol. 12, 1146 (1975).
- D. Kern, "Optimization of Electron Probe Forming Systems with Respect to Aberration and Vertical Beam Landing," J. Vac. Sci. Technol. 16, 1686 (1979).
- E. Munro and H. C. Chu, "Numerical Analysis of Electron Beam Lithography Systems," *Optik* 60, 371 (1981/82); 61, No. 1, 1 (1982); 61, No. 2, 121 (1982); 61, No. 3, 213 (1982).
- C. H. Schaefer, "A Theoretical Performance Comparison of Six Electrostatic E-Beam Deflectors," J. Vac. Sci. Technol. B 4, 1237 (1986).
- H. C. Pfeiffer and G. O. Langner, "Advanced Deflection Concept for Large Area, High Resolution E-Beam Lithography," J. Vac. Sci. Technol. 19, 1058 (1981).
- E. Goto, T. Soma, M. Idesawa, and T. Sasaki, "In-Lens Deflection System with Nonequisectored-Type Multipole Electrostatic Deflectors," J. Vac. Sci. Technol. B 1, 1289 (1983).
- M. A. Sturans and H. C. Pfeiffer, "Variable Axis Immersion Lens (VAIL)," Proceedings of Microcircuit Engineering 83, H. Ahmed, J. R. A. Cleaver, and G. A. C. Jones, Eds., Academic Press, Inc., New York, 1983.
- D. P. Kern, M. A. Sturans, H. C. Pfeiffer, and W. Stickel, "Computer Analysis of VAIL," Proceedings of Microcircuit Engineering 84, A. Heuberger and H. Beneking, Eds., Academic Press, Inc., New York, 1985, p. 185.
- 57. G. L. Varnell, D. F. Spicer, A. C. Rodger, and R. D. Holland, "High Speed Pattern Generation," Proceedings of the 6th International Conference on Electron and Ion Beam Science and Technology, R. Bakish, Ed., Electrochemical Society, Pennington, NJ, 1974, p. 97.
- A. N. Broers, "Koehler Illumination and Brightness Measurements with Lanthanum Hexaboride Cathodes," J. Vac. Sci. Technol. 16, 1692 (1979).
- D. P. Kern, R. Viswanathan, R. H. Naumann, and T. H. P. Chang, "A Round Beam Exposure System with Multiple Beam Sizes," Proceedings of the 10th International Conference on Electron and Ion Beam Science and Technology, R. Bakish, Ed., Electrochemical Society, Pennington, NJ, 1982, p. 15.
- H. C. Pfeiffer, "Variable Spot Shaping for Electron Beam Lithography," J. Vac. Sci. Technol. 15, 883 (1978).
- E. Goto, T. Soma, and M. Idesawa, "Design of a Variable-Aperture Projection and Scanning System for Electron Beam," J. Vac. Sci. Technol. 15, 883 (1978).
- M. G. R. Thompson, R. J. Collier, and D. R. Harriot, "Double-Aperture Method of Producing Variable Shaped Writing Spots for Electron Lithography," J. Vac. Sci. Technol. 15, 891 (1978).
- 63. H. C. Pfeiffer, "Basic Limitations of Probe Forming Systems Due to Electron-Electron Interactions" Proceedings of the 5th Annual SEM Symposium, O. Johari, Ed., Illinois Institute of Technology Research Institute, Chicago, 1972, p. 113.
- T. R. Groves, D. L. Hammond, and H. Kuo, "Electron Beam Broadening by Discreteness of Space Charge," J. Vac. Sci. Technol. 16, 1680 (1979).
- 65. T. H. P. Chang, "Proximity Effects in Electron Beam Lithography," J. Vac. Sci. Technol. 12, 1271 (1975).
- M. Parikh and D. F. Kyser, "Energy Deposition Functions in Electron Resist Films on Substrates," J. Appl. Phys. 50, 1104 (1979).
- 67. G. Owen, P. Rissman, and M. Long, "Application of the GHOST Proximity Effect Correction Scheme to Round Beam and Shaped Beam Electron Beam Lithography Systems," J.

- Vac. Sci. Technol. B 3, 153 (1985).
- S. A. Rishton and D. P. Kern, "Point Exposure Distribution Measurements for Proximity Correction in Electron Beam Lithography on a Sub-100 nm Scale," *J. Vac. Sci. Technol. B* 5, 135 (1987).
- G. Möllenstedt and R. Speidel, "Elektonenoptischer Mikroschreiber unter elektronenmikroskopischer Arbeitskontrolle," *Physikalische Blätter* 16, 192 (1960).
- A. N. Broers, "Combined Electron and Ion Beam Processes for Microelectronics," Microelectron. & Reliabil. 4, 103 (1965).
- 71. T. H. P. Chang and W. C. Nixon, "Electron Beam Formation of 800 Å Wide Al Lines," J. Sci. Instrum. 44, 231 (1967).
- A. N. Broers, W. W. Molzen, J. J. Cuomo, and N. D. Wittels, "Electron-Beam Fabrication of 80 Angstrom Metal Structures," Appl. Phys. Lett. 29, 596 (1976).
- I. Haller, M. Hatzakis, and R. Srinivasan, "High-Resolution Positive Resists for Electron-Beam Exposure," IBM J. Res. Develop. 12, 251 (1968).
- S. P. Beaumont, T. Tamamura, and C. D. W. Wilkinson, "A Two Layer Resist System for Efficient Liftoff in Very High Resolution Electron Beam Lithography," *Proceedings of Microcircuit Engineering 80*, Delft University Press, Netherlands, 1981, p. 381.
- A. N. Broers, "Resolution Limits of PMMA Resist for Exposure with 50kV Electrons," J. Electrochem. Soc.: Solid State Sci. & Technol. 128, 166 (1981).
- S. A. Rishton, H. Schmid, D. P. Kern, H. E. Luhn, T. H. P. Chang, G. A. Sai-Halasz, M. R. Wordeman, E. Ganin, and M. Polcari, "Lithography for Ultra Short Channel Silicon FET Circuits," J. Vac. Sci. Technol. B 6, 140 (1988).
- P. W. Whipps, "Negative Electron Resists Based on Polystyrene," *Proceedings of Microcircuit Engineering 83*, H. Ahmed, J. R. A. Cleaver, and G. A. C. Jones, Eds., Academic Press, Inc., New York, 1983.
- S. Thoms, I. McIntyre, S. P. Beaumont, M. A1 Mudares, and C. D. W. Wilkinson, "Fabrication of Quantum Wires in GaAs/ AlGaAs Heterolayers," *J. Vac. Sci. Technol. B* 6, 127 (January/ February 1988).
- B. Singh, S. P. Beaumont, P. G. Bower, and C. D. W. Wilkinson, "New Inorganic Electron Resist System for High Resolution Lithography," *Appl. Phys. Lett.* 41, 889 (1982).
- B. Singh, S. P. Beaumont, P. G. Bower, and C. D. W. Wilkinson, "Sub-50-nm Lithography in Amorphous Se-Ge Inorganic Resist by Electron Beam Exposure," *Appl. Phys. Lett.* 41, 1002 (1982).
- A. N. Broers and M. Pomerantz, "Rapid Writing of Fine Lines in Langmuir-Blodgett Films Using Electron Beams," *Thin Solid Films* 99, 323 (1983).
- M. Isaacson and A. Muray, "In Situ Vaporization of Very Low Molecular Weight Resists Using ½ nm Diameter Electron Beams," J. Vac. Sci. Technol. 19, 1117 (1981).
- A. Muray, M. Scheinfein, M. Isaacson, and I. Adesida, "Radiolysis and Resolution Limits of Inorganic Halide Resists," J. Vac. Sci. Technol. B 3, 367 (1985).
- M. E. Mochel, C. J. Humphreys, J. A. Eades, J. M. Mochel, and A. M. Petford, "Electron Beam Writing on a 20 Angstrom Scale in Metal Beta-Aluminas," *Appl. Phys. Lett.* 42, 392 (1983)
- E. Kratschmer and M. Isaacson, "Nanostructure Fabrication in Metals, Insulators, and Semiconductors Using Self-Developing Metal Inorganic Resist," J. Vac. Sci. Technol. B 4, 361 (1986).
- F. Emoto, K. Gamo, S. Namba, N. Samoto, and R. Shimizu, "8 nm Wide Line Fabrication in PMMA on Si Wafers by Electron Beam Exposure," *Jpn. J. Appl. Phys.* 24, 5 (1985).
- 87. S. P. Beaumont, B. Singh, and C. D. W. Wilkinson, "Very High Resolution Electron Beam Lithography—Thin Films, or Solid Substrates?" Proceedings of the 10th International Conference on Electron and Ion Beam Science and Technology, R. Bakish, Ed., Electrochemical Society, Pennington, NJ, 1982, p. 112.
- H. G. Craighead, R. E. Howard, L. D. Jackel, and P. M. Mankiewich, "10-nm Linewidth Electron Beam Lithography

489

- on GaAs," Appl. Phys. Lett. 42, 38 (1983).
- K. Murata, D. F. Kyser, and C. H. Ting, "Monte Carlo Simulation of Fast Secondary Electron Production in Electron Beam Resists," J. Appl. Phys. 52, 4396 (1981).
 S. A. Rishton, "Resolution Limits in Electron Beam
- S. A. Rishton, "Resolution Limits in Electron Beam Lithography," Ph.D. Thesis, Glasgow University, Scotland, 1984
- S. A. Rishton, S. P. Beaumont, and C. D. W. Wilkinson, "Exposure Range of Low Energy Electrons in PMMA," Proceedings of the 10th International Conference on Electron and Ion Beam Science and Technology, R. Bakish, Ed., Electrochemical Society, Pennington, NJ, 1982, p. 211.
- S. A. Rishton, S. P. Beaumont, and C. D. W. Wilkinson, "Measurement of the Effect of Secondary Electrons on the Resolution Limit of PMMA," Proceedings of Microcircuit Engineering 82, Grenoble, France, 1982, p. 341.
- V. K. Sharma, S. Affrossman, and R. A. Pethrick, "Electron Beam Lithography—Influence of Molecular Characteristics on the Performance of Positive Resists," *Brit. Polym. J.* 16, 73 (1984).
- J. D. Ferry, Viscoelastic Properties of Polymers, John Wiley & Sons, Inc., New York, 1980.
- T. H. P. Chang, A. D. Wilson, A. J. Speth, and C. H. Ting, "Vector-Scan I: An Automated Electron Beam System for High Resolution Lithography," Proceedings of the 7th International Conference on Electron and Ion Beam Science and Technology, R. Bakish, Ed., Electrochemical Society, Pennington, NJ, 1976, p. 392
- A. D. Wilson, A. Kern, A. J. Speth, A. M. Patlach, P. R. Jaskar, T. W. Studwell, and W. L. Keller, "Automation of Vector Scan I Electron Beam Lithographic System,"
 Proceedings of the 7th International Conference on Electron and Ion Beam Science and Technology, R. Bakish, Ed., Electrochemical Society, Pennington, NJ, 1976, p. 361.
- S. A. Rishton, S. P. Beaumont, and C. D. W. Wilkinson, "Measurement of the Profile of Finely Focused Electron Beams in a Scanning Electron Microscope," J. Phys. E: Sci. Instrum. 17, 296 (1984).
- J. Melngailis, "Focused Ion Beam Technology and Applications," J. Vac. Sci. Technol. B 5, 469 (1987).
- R. Levi-Setti, G. Crow, and Y. L. Wang, "Progress in High Resolution Scanning Ion Microscopy and Secondary Ion Mass Spectroscopy Imaging Microanalysis," Scanning Electron Microsc. 2, 535 (1985).
- T. Kato, H. Morimoto, K. Saitoh, and H. Nakata, "Submicron Pattern Fabrication by Focussed Ion Beams," J. Vac. Sci. Technol. B 3, 50 (1985).
- Y. Ochiai, S. Matsui, and K. Mori, "Focused Ion Beam Technology," Solid State Technol. 30, 75-79 (November 1987).
- 102. R. L. Kubena, R. J. Joyce, J. W. Ward, H. L. Garvin, F. P. Stratton, and R. G. Brault, "Dot Lithography for Zero-Dimensional Quantum Wells Using Focused Ion Beams," J. Vac. Sci. Technol. B 6, 353 (1988).
- 103. E. Miyauchi, T. Morita, A. Takamori, H. Arimoto, Y. Bamba, and H. Hashimoto, "Maskless Ion Beam Writing of Precise Doping Patterns with Be and Si for Molecular Beam Epitaxially Grown Multilayer GaAs," J. Vac. Sci. Technol. B 4, 189 (1986).
- 104. G. L. R. Mair and T. Muley, "Ion Beam Lithography," Microelectron. Eng. 3, 133 (1985).
- J. Orloff and L. W. Swanson, "Angular Intensity of a Gas-Phase Field Ionization Source," J. Appl. Phys. 50, 6026 (1979).
- 106. R. J. Blackwell, J. A. Kubby, G. N. Lewis, and B. M. Siegel, "Experimental Focused Ion Beam System Using a Gaseous Field Ion Source," J. Vac. Sci. Technol. B 3, 82 (1985).
- T. Itakura, K. Horiuchi, and S. Yamamoto, "Focusing Column for Helium Field Ion Source," *Microelectron. Eng.* 3, 153 (1985).
- G. Binnig, H. Rohrer, Ch. Gerber, and E. Weibel, "Surface Studies by Scanning Tunneling Microscopy," *Phys. Rev. Lett.* 49, 47 (1982).

- M. A. McCord and R. F. W. Pease, "Lift-Off Metalization Using PMMA Exposed with a Scanning Tunneling Microscope," J. Vac. Sci. Technol. B 4, 86 (1986).
- 110. E. E. Ehrichs, R. M. Silver, and A. L. de Lozanne, "Direct Writing with the STM," Proceedings of the 2nd International Conference on Scanning Tunneling Microscopy/Spectroscopy, Oxnard, CA, 1987 (to be published in J. Vac. Sci. Technol., March/April 1988).
- 111. U. Staufer, R. Wiesendanger, L. Eng, L. Rosenthaler, H. R. Hidber, and H.-J. Guntherodt, "Surface Modification in the Nanometer Range by the Scanning Tunneling Microscope," Proceedings of the 2nd International Conference on Scanning Tunneling Microscopy/Spectroscopy, Oxnard, CA, 1987 (to be published in J. Vac. Sci. Technol., March/April 1988).
- 112. R. S. Becker, J. A. Golovchenko, and B. S. Swartzentruber, "Atomic-Scale Surface Modifications Using a Tunnelling Microscope," *Nature* 325, 419 (1987).
- 113. K. A. Rao, L. W. Swanson, and A. E. Bell, "Application of the STM-LMIS to Microstructure Fabrication," J. Vac. Sci. Technol. B 6, 306 (1988).
- 114. M. A. McCord and R. F. W. Pease, "High Resolution, Low-Voltage Probes from a Field Emission Source Close to the Target Plane," J. Vac. Sci. Technol. B 3, 198 (1985).
- 115. H. Rarback, D. Shu, S. C. Feng, H. Ade, J. Kirz, I. McNulty, D. P. Kern, T. H. P. Chang, Y. Vladimirsky, N. Iskander, D. Attwood, K. McQuaid, and S. Rothman, "A Scanning X-Ray Microscope with 75 nm Resolution," *Rev. Sci. Instrum.* 59, 52 (1988).
- X-ray source 1: C. Jacobsen and H. Rarback, "Predictions on the Performance of the Soft X-Ray Undulator," *International* Conference on Insertion Devices for Synchrotron Sources, SPIE Proc. 582, 201 (1986); X-ray source 2: "1-2 GeV Synchrotron Radiation Source," PUB-5172 Rev., Lawrence Berkeley Laboratory, University of California, Berkeley, July 1986.
- M. P. Lepselter, "Scaling the Micron Barrier with X-Rays," *IEDM Tech. Digest*, p. 42 (December 8-10, 1980).
- 118. H. I. Smith, D. L. Spears, and S. E. Bernacki, "X-Ray Lithography: A Complementary Technique to Electron Beam Lithography," J. Vac. Sci. Techol. 10, 913 (1973).
- 119. B. Leslie, A. Neukermans, T. Simon, and J. Foster, "Enhanced Brightness X-Ray Source," J. Vac. Sci. Technol. B 1, 1251 (1983).
- D. C. Flanders, "Replication of 174 Å Lines and Spaces in Polymethylmethacrylate Using X-Ray Lithography," Appl. Phys. Lett. 36, 93 (1980).
- 121. E. H. Anderson, D. P. Kern, and H. I. Smith, "Fabrication by Tri-Level Electron Beam Lithography of X-ray Masks with 50 nm Linewidths, and Replication by X-Ray Nanolithography," *Microelectron. Eng.* 6, 541 (1987).
- I. Okada, Y. Saitoh, S. Itabashi, and H. Yoshihara, "A Plasma X-Ray Source for X-Ray Lithography," J. Vac. Sci. Technol. B. 4, 243 (1986).
- 123. M. Kuehne and H.-C. Petzold, "Conversion Efficiency of Laser Radiation into Soft X-Ray Radiation of Laser Produced Plasmas for X-Ray Lithography," *Microelectron. Eng.* 3, 565
- J. Eberle, H. Krompholz, R. Lebert, W. Neff, and R. Noll, "Plasma Focus as a Radiation Source for X-Ray Lithography," Microelectron. Eng. 3, 611 (1985).
- N. Atoda, H. Kawakatsu, H. Tanino, S. Ichimura, M. Hirata, and K. Hoh, "Diffraction Effects on Pattern Replication with Synchrotron Radiation," J. Vac. Sci. Technol. B 1, 1267 (1983).
- 126. H. Betz, K. Heinrich, A. Heuberger, H. Huber, and H. Oertel, "Resolution Limits in X-Ray Lithography Calculated by Means of X-Ray Lithography Simulator XMAS," J. Vac. Sci. Technol. B 4, 248 (1986).
- A. Heuberger, "X-Ray Lithography," Microelectron. Eng. 5, 3 (1986).
- 128. R. P. Haelbich, J. P. Silverman, W. D. Grobman, J. R. Maldonado, and J. M. Warlaumont, "Design and Performance of an X-Ray Lithography Beam Line at a Storage Ring," J.

- Vac. Sci. Technol. B 1, 1262 (1983).
- 129. K. Hoh, "Present State of High Resolution X-Ray Lithography with Synchrotron Radiation," Proceedings of Microcircuit Engineering 84, A. Heuberger and H. Beneking, Eds., Academic Press, Inc., New York, 1985, p. 283.
- R. Feder, E. Spiller, and J. Topalian, "X-Ray Lithography," Polym. Eng. Sci. 17, 385 (1977).
- 131. R. Ward, A. R. Franklin, I. H. Lewin, P. A. Gould, and M. J. Plummer, "A 1:1 Electron Stepper," J. Vac. Sci. Technol. B 4, 89 (1986).
- 132. I. Mori, K. Sugihara, C. Itoh, M. Tabata, and T. Shinozaki, "An Electron Beam Image Projection System with Automatic Wafer Handling," *Microelectron. Eng.* 3, 69 (1985).
- 133. H. Bohlen, J. Greschner, J. Keyser, W. Kulcke, and P. Nehmiz, "Electron-Beam Proximity Printing—A New High-Speed Lithography Method for Submicron Structures," *IBM J. Res. Develop.* 26, 568 (1982).
- 134. W. Zapka, P. Nehmiz, U. Behringer, W. Haug, J. Keyser, and H. Bohlen, "Electron Beam Proximity Printing: Step and Scan Technique for Future Small Groundrule Lithography," Proceedings of Microcircuit Engineering 84, A. Heuberger and H. Beneking, Eds., Academic Press, Inc., New York, 1985, p. 265.
- H. Koops, "On Electron Projection Systems," J. Vac. Sci. Technol. 10, 909 (1973).
- 136. M. B. Heritage, "Electron-Projection Microfabrication System," J. Vac. Sci. Technol. 12, 1135 (1975).
- J. Frosien, B. Lischke, and K. Anger, "Aligned Multilayer Structure Generation by Electron Microprojection," J. Vac. Sci. Technol. 16, 1827 (1979).
- 138. J. Grob, H. Koops, and G. Westermann, "Electron Beam Reducing Image Projection with Variable Scale," Proceedings of Microcircuit Engineering 84, A. Heuberger and H. Beneking, Eds., Academic Press, Inc., New York, 1985, p. 137.
- I. Adesida, E. Kratschmer, E. D. Wolf, A. Muray, and M. Isaacson, "Ion Beam Lithography at Nanometer Dimensions," J. Vac. Sci. Technol. B 3, 45 (1985).
- 140. L. Karapiperis, D. Dubreuil, Ph. David, and D. Dieumegard, "Ion Beam Lithography: An Investigation of Resolution Limits and Sensitivities of Ion-Beam Exposed PMMA," J. Vac. Sci. Techol. B 3, 353 (1985).
- M. D. Giles, R. K. Watts, and E. Labate, "Ultimate Resolution and Contrast in Ion-Beam Lithography," J. Vac. Sci. Technol. B 5, 1588 (1987).
- 142. J. N. Randall, D. C. Flanders, N. P. Economou, J. P. Donnelly, and E. I. Bromley, "Silicon Nitride Stencil Masks for High Resolution Ion Lithography Proximity Printing," J. Vac. Sci. Technol. B 1, 1152 (1983).
- 143. J. N. Randall, D. C. Flanders, N. P. Economou, J. P. Donnelly, and E. I. Bromley, "Masked Ion Beam Resist Exposure Using Grid Support Stencil Masks," J. Vac. Sci. Technol. B 3, 58 (1985).
- 144. D. B. Rensch, R. L. Seliger, G. Csanky, R. D. Olney, and H. L. Stover, "Ion-Beam Lithography for IC Fabrication with Submicrometer Features," J. Vac. Sci. Technol. 16, 1897 (1979)
- L. Csepregi, F. Iberl, and P. Eichinger, "Ion-Beam Shadow Printing Through Thin Silicon Foils Using Channeling," Appl. Phys. Lett. 37, 630 (1980).
- J. L. Bartelt, "Masked Ion Beam Lithography: An Emerging Technology," Solid State Technol. 29, 215 (May 1986).
- 147. R. Fischer, E. Hammel, H. Löschner, G. Stengl, and P. Wolf, "Ion Projection Lithography in (IN)organic Resist Layers," *Microelectron. Eng.* 5, 193 (1986).
- 148. R. H. Dennard, F. H. Gaensslen, L. Kuhn, and H. N. Yu, "Design of Micron MOS Switching Devices," *IEDM Tech. Digest*, p. 344 (1972).
- 149. G. Baccarani and M. R. Wordeman, "Transconductance Degradation in Thin-Oxide MOSFET's," *IEEE Trans. Electron Devices* ED-30, 1295 (1983).
- 150. J. P. Leburton and G. Dorda, "Effect of Electron Temperature on the Gate-Induced Charge in Small Size MOS Transistors,"

- Solid State Electron. 26, 611 (1983).
- J. G. Ruch, "Electron Dynamics in Short Channel Field Effect Transistors," *IEEE Trans. Electron Devices* ED-19, 652 (1972).
- 152. G. Baccarani, M. R. Wordeman, and R. H. Dennard, "Generalized Scaling Theory and Its Application to a ¼ Micrometer MOSFET Design," *IEEE Trans. Electron Devices* ED-31, 452 (1984).
- 153. G. A. Sai-Halasz, M. R. Wordeman, D. P. Kern, E. Ganin, S. Rishton, D. S. Zicherman, H. Schmid, M. R. Polcari, H. Y. Ng, P. J. Restle, T. H. P. Chang, and R. H. Dennard, "Design and Experimental Technology for 0.1μm Gate-Length Low-Temperature Operation FET's," Electron Device Lett. EDL-8, 463 (1987).
- 154. G. A. Sai-Halasz, "Fast Switching Times in 0.1 μm Gate Length FETs," preprint; available from G. A. Sai-Halasz, IBM Thomas J. Watson Research Center, P. O. Box 218, Yorktown Heights, NY 10598.
- 155. P. C. Chao, P. M. Smith, K. H. G. Duh, J. M. Ballingall, L. F. Lester, B. R. Lee, A. A. Jabra, and R. C. Tiberio, "High Performance 0.1μm Gate-Length Planar-Doped HEMTs," *IEDM Tech. Digest*, p. 410 (1987).
- 156. G. A. Sai-Halasz, "Observation of Velocity Overshoot in Short-Channel NMOS Devices," preprint; available from G. A. Sai-Halasz, IBM Thomas J. Watson Research Center, P.O. Box 218, Yorktown Heights, NY 10598.
- 157. S. Y. Chou, D. A. Antoniadis, and H. I. Smith, "Observation of Electron Velocity Overshoot in Sub-100-nm-Channel MOSFET's in Silicon," *Electron Device Lett.* EDL-6, 665 (1985).
- 158. G. G. Shahidi, D. A. Antoniadis, and H. I. Smith, "Electron Velocity Overshoot at 300 K and 77 K in Silicon MOSFET's with Submicron Channel Lengths," *IEDM Tech. Digest*, p. 824 (1986)
- 159. G. Möllenstedt, H. Schmid, and H. Lichte, "Measurement of the Phase Shift Between Electron Waves Due to a Magnetic Flux Enclosed in a Metallic Cylinder," Proceedings of the 10th International Congress on Electron Microscopy, Hamburg, W. Germany, 1982, p. 433.
- 160. R. Doll and M. Näbauer, "Experimental Proof of Magnetic Flux Quantization in a Superconducting Ring," Phys. Rev. Lett. 7, 51 (1961).
- S. Washburn and R. A. Webb, "Aharonov-Bohm Effect in Normal Metal Quantum Coherence and Transport," Adv. Phys. 35, 375 (1986).
- 162. C. P. Umbach, C. van Haesendonck, R. B. Laibowitz, S. Washburn, and R. A. Webb, "Direct Observation of the Stochastic Self-Averaging of the Aharonov-Bohm Effect in Normal Metals," *Phys. Rev. Lett.* 56, 386 (1986).
- 163. H. Schmid, "Coherence Length Measurement by Producing Extremely High Phase Shifts," Proceedings of the 8th European Congress on Electron Microscopy, Budapest, Hungary, 1984, p. 285.
- 164. S. Washburn, H. Schmid, D. Kern, and R. A. Webb, "Normal-Metal Aharonov-Bohm Effect in the Presence of a Transverse Electric Field," Phys. Rev. Lett. 59, 1791 (1987).
- S. Washburn, "Fluctuations in the Extrinsic Conductivity of Disordered Metal," IBM J. Res. Develop. 32, 335-346 (1988).
- 166. H. Haucke, A. D. Benoit, C. P. Umbach, S. Washburn, H. Schmid, D. Kern, and R. A. Webb, "Direct Observation of Non-Local Conductance Fluctuations," preprint; available from H. Haucke, IBM Thomas J. Watson Research Center, P.O. Box 218, Yorktown Heights, NY 10598.
- 167. S. Washburn, A. B. Fowler, H. Schmid, and D. Kern, "Possible Observation of Transmission Resonances in GaAs-Al_xGa_{1-x}As Transistors," preprint; available from S. Washburn, IBM Thomas J. Watson Research Center, P.O. Box 218, Yorktown Heights, NY 10598.
- 168. S. Laux and F. Stern, "Electron States in Narrow Gate-Induced Channels in Si," Appl. Phys. Lett. 49, 91 (1986).
- 169. T. P. Smith III, H. Arnot, C. M. Knoedler, S. E. Laux, and H. Schmid, "Capacitance Oscillations in One-Dimensional Electron Systems," *Phys. Rev. Lett.* 59, 2802 (1987).

- 170. T. P. Smith III, K. Y. Lee, J. M. Hong, C. M. Knoedler, and D. P. Kern, "Electronic Spectroscopy of Zero-Dimensional Systems," preprint; available from T. P. Smith III, IBM Thomas J. Watson Research Center, P.O. Box 218, Yorktown Heights, NY 10598.
- 171. C. M. Knoedler and T. F. Kuech, "Selective GaAs/Al_xGa_{1-x}As Reactive Ion Etching Using CCl₂F₂," J. Vac. Sci. Technol. B 4, 1233 (1986).
- 172. T. Nishino, M. Miyake, Y. Harada, and U. Kawabe, "Three-Terminal Superconducting Device Using a Si Single-Crystal Film," *Electron Device Lett.* EDL-6, 297 (1985).
- T. Kawakami and H. Takayanagi, "Single-Crystal N-InAs Coupled Josephson Junction," Appl. Phys. Lett. 46, 92 (1985).
- 174. H. Takayanagi and T. Kawakami, "Superconducting Proximity Effect in the Native Inversion Layer on InAs," *Phys. Rev. Lett.* 54, 2449 (1985).
- 175. A. W. Kleinsasser, T. N. Jackson, G. D. Pettit, H. Schmid, J. M. Woodall, and D. P. Kern, "N-InAs/GaAs Heterostructure Superconducting Weak Links with Nb Electrodes," Appl. Phys. Lett. 49, 1741 (1986).
- 176. K. K. Likharev, "The Relation J_s (φ) for SNS Bridges of Variable Thickness," Sov. Tech. Phys. Lett. 2, 12 (1976).
- 177. J. F. Smyth, S. Schultz, D. Kern, H. Schmid, and D. Yee, "Hysteresis and FMR of Submicron Permalloy Particulate Arrays," Proceedings of the 32nd Annual Conference on Magnetism & Magnetic Materials, J. Appl. Phys. 63 (April 1988).
- 178. "High Resolution X-Ray Optics," SPIE Proc. 316 (1981).
- 179. P. J. Coane, D. P. Kern, A. J. Speth, and T. H. P. Chang, "An E-Beam Lithography System for Microfabrication of Structures with Minimum Dimensions Below 1000 Å," *Proceedings of Microcircuit Engineering 82*, Grenoble, France, 1982, p. 373.
- 180. V. Bögli and H. Beneking, "Nanometer Scale Device Fabrication in a 100 keV E-Beam System," Proceedings of Microcircuit Engineering 85, North-Holland Publishing Co., Amsterdam, 1985, p. 117.
- H. Aritome and S. Namba, "Fabrication of X-Ray Optical Elements by Electron Beam Lithography," SPIE Proc. 733, 440 (1986).
- 182. D. Kern, P. Coane, R. Acosta, T. H. P. Chang, R. Feder, P. Houzego, W. Molzen, J. Powers, A. Speth, R. Viswanathan, J. Kirz, H. Rarback, and J. Kenney, "Electron Beam Fabrication and Characterization of Fresnel Zone Plates for Soft X-Ray Microscopy," SPIE Proc. 447, 204 (1983).
- Y. Vladimirsky, E. Källne, and E. Spiller, "Fabrication of Freestanding Transmission Grating and Zone Plates," SPIE Proc. 448, 25 (1984).
- 184. C. J. Buckley, M. T. Browne, and P. Charalambous, "Contamination Lithography for the Fabrication of Zone Plate X-Ray Lenses," SPIE Proc. 537, 213 (1985).
- 185. Y. Vladimirsky, D. P. Kern, T. H. P. Chang, D. T. Attwood, H. Ade, J. Kirz, I. McNulty, H. Rarback, and D. Shu, "High Resolution Fresnel Zone Plates for X-Rays," J. Vac. Sci. Technol. B 6, 311 (1988).
- X-Ray Microscopy, G. Schmahl and D. Rudolph, Eds., Springer-Verlag, Berlin, 1984.
- X-Ray Microscopy—Instrumentation and Biological Applications, P. C. Cheng and G. J. Jan, Eds., Springer-Verlag, Berlin, 1984.
- 188. "Science with Soft X-Rays," F. J. Himpsel and R. W. Klaffky, Eds., SPIE Proc. 447 (1984).
- 189. H. Ade, J. Kirz, H. Rarback, S. Hulbert, E. Johnson, D. Kern, T. H. P. Chang, and Y. Vladimirsky, "Possibilities for a Scanning Photoemission Microscope at the NSLS," Proceedings of the International Symposium on X-Ray Microscopy, Brookhaven, NY, Springer-Verlag, Heidelberg, 1987
- T. Fujita, H. Nishihara, and J. Koyama, "Fabrication of Micro Lenses Using Electron-Beam Lithography," Opt. Lett. 6, 613 (1981).
- T. Shiono, K. Setsune, O. Yamazaki, and K. Wasa, "Rectangular-Apertured Micro-Fresnel Lens Arrays Fabricated

- by Electron-Beam Lithography," Appl. Opt. 26, 587 (1987).
- T. Fujita, H. Nishihara, and J. Koyama, "Blazed Gratings and Fresnel Lenses Fabricated by Electron-Beam Lithography," Opt. Lett. 7, 578 (1982).
- 193. K. Tatsumi, T. Saheki, T. Takei, and K. Nukui, "High-Performance Micro-Fresnel Lens Fabricated by UV Lithography," Appl. Opt. 23, 1742 (1984).
- 194. L. B. Lesem, P. M. Hirsch, and J. A. Jordan, Jr., "The Kinoform: A New Wavefront Reconstruction Device," *IBM J. Res. Develop.* 13, 150 (1969).
- 195. M. S. Cohen, E. Kratschmer, Y. Vladimirsky, T. H. P. Chang, D. P. Kern, and E. G. Lean, "Fresnel Zone Plates for Magneto-Optic Recording," Research Report RC-13389, IBM Thomas J. Watson Research Center, Yorktown Heights, NY, 1987.

Received February 8, 1988; accepted for publication February 21, 1988 T. H. Philip Chang IBM Research Division, T. J. Watson Research Center, P.O. Box 218, Yorktown Heights, New York 10598. Dr. Chang received the B.A. degree and the Ph.D. degree in electrical sciences from Cambridge University, England, in 1963 and 1967, respectively. In 1971 he joined the IBM Thomas J. Watson Research Center, where he has been engaged in research in electron-beam technology, microfabrication, high-resolution lithography, and, more recently, the nanostructure technology program.

Dieter P. Kern IBM Research Division, T. J. Watson Research Center, P.O. Box 218, Yorktown Heights, New York 10598. Dr. Kern is currently manager of Nanostructure Fabrication in the Semiconductor Science and Technology Department. He joined IBM in 1978 as a visiting scientist in the Applied Research Department, working on electron-optical design, modeling of development and etching processes, proximity-effect correction in electron-beam lithography, electron-beam testing, and high-resolution electron-beam fabrication. In 1982 he became manager of Advanced Electron-Beam Lithography, and in 1983 manager of Electron-Beam Testing and Microfabrication. Dr. Kern received a Diplom degree in physics from the University of Tübingen, West Germany, in 1970, and a Ph.D. in physics (summa cum laude) from Tübingen University in 1978. He is a member of the American Physical Society and the German Society for Electron Microscopy.

Ernst Kratschmer IBM Research Division, T. J. Watson Research Center, P.O. Box 218, Yorktown Heights, New York 10598. Dr. Kratschmer joined IBM as a visiting scientist in 1986. He is currently involved in research and development of high-resolution electron-beam lithography systems. Prior to joining IBM, he was a research associate at the National Research and Resource Facility for Submicron Structures at Cornell University, Ithaca, New York, where he was exploring the use of an STEM for lithography in organic and inorganic resists. Dr. Kratschmer received his Dr.-Ing. from Rheinisch Westfälische Technische Hochschule, Aachen University, Aachen, West Germany, in 1982. He is a member of the American Vacuum Society.

Kim Y. Lee IBM Research Division, T. J. Watson Research Center, P.O. Box 218, Yorktown Heights, New York 10598. Dr. Lee graduated B.Sc. and Ph.D. in electronics and electrical engineering from the University of Glasgow, United Kingdom, in 1983 and 1987, respectively. His Ph.D. dissertation concerned the fabrication of ultrasmall GaAs FET devices using electron-beam lithography. Dr. Lee joined IBM in 1987 as a visiting scientist. His current research involves the application of nanolithographic techniques to fabricate GaAs/GaAlAs quantum devices.

Hans E. Luhn IBM Research Division, T. J. Watson Research Center, P.O. Box 218, Yorktown Heights, New York 10598. Mr. Luhn graduated from the Carl-Duisberg-Schule in Wuppertal, West Germany in 1951, and studied business administration in Remscheid, West Germany. He joined the Research Division at the IBM Thomas J. Watson Research Center in 1956. Mr. Luhn then studied physics at Fairleigh Dickinson University, Teaneck, New Jersey, and at Bridgeport University, Bridgeport, Connecticut. He has been a member of the electron-beam microfabrication program since 1972, and is currently a Senior Associate Engineer with the Nanostructure Fabrication group, where his primary responsibilities are in the areas of system development and process studies.

Mark A. McCord IBM Research Division, T. J. Watson Research Center, P.O. Box 218, Yorktown Heights, New York 10598. Dr. McCord joined IBM on a postdoctoral assignment after receiving his Ph.D. from Stanford University in 1987. At Stanford he worked on lithographic applications of the scanning tunneling microscope. At IBM he is continuing research on applications of the STM as well as working on other aspects of nanotechnology.

Stephen A. Rishton IBM Research Division, T. J. Watson Research Center, P.O. Box 218, Yorktown Heights, New York 10598. Dr. Rishton received his Ph.D. in electronic engineering from the University of Glasgow in 1984, and his B.Sc.(Eng.) degree from University College, London, in 1980, also in electronic engineering. He first worked at the IBM Thomas J. Watson Research Center as a summer student in 1979, and returned on a postdoctoral assignment in 1984 to do research on nanolithographic equipment and techniques. He became a Research Staff Member in 1987. Dr. Rishton has worked on the fabrication of various ultrasmall structures and on electron-beam lithography on the hundredthmicron scale; he is currently involved in the fabrication of tenthmicron silicon FET circuits.

Yuli Vladimirsky IBM General Technology Division, East Fishkill facility, Route 52, Hopewell Junction, New York 12533. Dr. Vladimirsky was a Research Scientist at the Lawrence Berkeley Laboratory from 1984 until recently, working with the Nanostructure Fabrication group at the IBM Thomas J. Watson Research Center on the development of imaging optics for soft X-ray synchrotron radiation. Since 1981 he has worked on research and development of submicron photo-, X-ray, and electron-beam lithography techniques for fabrication of deep UV and soft X-ray optical elements. He received his M.S. in physics of metals in 1964 and his Ph.D. in physics and mathematics in 1970 from the Leningrad Polytechnic Institute. After completion of his studies Dr. Vladimirsky conducted research on defects, radiation damage, X-ray luminescence, and other irradiation effects in solids, and experimental and theoretical investigations in X-ray optics, mosaic structure, and X-ray optical properties of crystals and pseudocrystals. Dr. Vladimirsky is a member of the American Association for the Advancement of Science, the American Physical Society, and the New York Academy of Sciences.